Structural rather than catalytic role for mitochondrial respiratory chain supercomplexes

Michele Brischigliaro[1,2,*,¶], Alfredo Cabrera-Orefice[3], Susanne Arnold[3,4,#], Carlo Viscomi[1,#], Massimo Zeviani[2,5,†,#], Erika Fernández-Vizarra[1,2,#,*, §]

[1] Department of Biomedical Sciences, University of Padova, Padova, Italy

[2] Veneto Institute of Molecular Medicine, Padova, Italy

[3] Radboud Institute for Molecular Life Sciences, Radboud University Medical Center, Nijmegen, The Netherlands

[4] Cologne Excellence Cluster on Cellular Stress Responses in Aging-Associated Diseases (CECAD), University of Cologne, Cologne, Germany

[5] Department of Neurosciences, University of Padova, Padova, Italy

* Correspondence to: Michele Brischigliaro (michele.brischigliaro@unipd.it) and Erika Fernández-Vizarra (erika.fernandezvizarra@unipd.it)

[#] Senior author

[§] Lead contact: Erika Fernandez-Vizarra

[¶] Present address: Department of Neurology, University of Miami Miller School of Medicine, Miami, FL, USA

[†] Present address: Institute for Maternal and Child Health, IRCCS “Burlo Garofolo”, Trieste, Italy

ABSTRACT

Mammalian mitochondrial respiratory chain (MRC) complexes are able to associate into quaternary structures named supercomplexes (SCs), which normally coexist with non-bound individual complexes. The functional significance of SCs has not been fully clarified and the debate has been centered on whether or not they confer catalytic advantages to the non-bound individual complexes. Mitochondrial respiratory chain organization does not seem to be conserved in all organisms. In fact, and differently from mammalian species, mitochondria from insect tissues are characterized by low amounts of SCs, despite the high metabolic demands and MRC activity shown by these mitochondria. Here, we show that attenuating the biogenesis of individual respiratory chain complexes was accompanied by increased formation of stable SCs, which are missing in *Drosophila melanogaster* in physiological conditions. This phenomenon was not accompanied by an increase in mitochondrial respiratory activity. Therefore, we conclude that SC formation is necessary to stabilize the complexes in suboptimal biogenetic conditions, but not for the enhancement of respiratory chain catalysis.

KEYWORDS: Mitochondrial respiratory chain, supercomplexes, respiratory chain complex biogenesis, mitochondrial respiratory activity

INTRODUCTION

Mitochondria are the organelles providing most of the cellular energy in form of adenosine triphosphate (ATP) in aerobic eukaryotes. The molecular machinery responsible for energy transformation is the oxidative phosphorylation (OXPHOS) system, which is canonically composed of five multiprotein complexes embedded in the inner mitochondrial membrane. OXPHOS consists of two tightly regulated processes: electron transport and ATP synthesis. Electron transport takes place between complexes I-IV and two mobile electron carriers (coenzyme Q and cytochrome *c*). During electron transport, complexes I, III and IV pump protons from the mitochondrial matrix to the intermembrane space, generating a proton gradient that provides the protonmotive force exploited by complex V to synthesize ATP. In mammalian mitochondria, mitochondrial respiratory chain (MRC) complexes I, III and IV can interact with each other forming supramolecular structures described generally by the term 'supercomplexes' [1,2]. MRC supercomplexes (SCs) can have different stoichiometries and compositions, ranging from the binding of only two complexes, such as the I_1III_2 and III_2IV_1 SCs [3,4], to higher-order associations between complexes I, III and IV, with the SC of $I_1III_2IV_1$ stoichiometry known as the 'respirasome' [1,5-9]. Now that the association of individual MRC complexes into supramolecular structures is well-established, with structures of several SC species being resolved, the debate is centered on what the functional significance of these structures might be.

Several possible roles have been proposed for SCs. First, it was suggested that the association between complex I (CI) and the obligate dimer of complex III ($CIII_2$) would allow substrate channeling, sequestering a dedicated coenzyme Q (CoQ) pool and allowing a more efficient electron transfer between the two complexes, while separating this electronic route from those of $FADH_2$-linked dehydrogenases (e.g. complex II) to the $CIII_2$ not bound to CI [1,10-15]. This increased efficiency would in turn decrease electron leak and, as a consequence, produce less reactive oxygen species (ROS) than the individual free complexes [16,17]. However, the available high-resolution respirasome structures show that the distance between the CoQ binding sites in CI and $CIII_2$ are too far apart to allow substrate channeling [4,18]. In addition, exogenously added CoQ was necessary to sustain CI activity in the purified I_1III_2 SC [3], arguing against a tightly bound and segregated CoQ pool as a functional component of the SC. A large body of work from the late 1960's to the 1980's, resulted in the 'random collision model' to explain electron transfer between the respiratory chain complexes, and in the evidence that CoQ is present as an undifferentiated pool[19-23]. More recently, additional proof of the non-compartmentalized

electronic routes from CI to $CIII_2$ and from complex II (CII) to $CIII_2$, came from kinetic measurements in sub-mitochondrial particles. In these systems, MRC organization in SCs was conserved but *b*- and *c*-type cytochromes in $CIII_2$ were equally accessible to CI-linked and CII-linked substrates [24], and CoQ reduced by CI in the respirasomes was able to reach and readily reduce external enzymes to the SCs [25]. In addition, growing evidence supports the notion that different MRC organizations exist *in vivo*, where varying proportions of SC vs. free complexes do not result in separate and distinct CI-linked and CII-linked respiratory activities [26-29]. This is in contrast with an idea that segregation into different types of SCs and in individual complexes to explains their functional interplay for the adaptation of OXPHOS activity [13]. The physical proximity of $CIII_2$ and CIV has also been suggested to promote faster electron transfer kinetics via cytochrome *c* [4,30,31], although this is a matter of debate as well [32,33].

The second main explanation to justify the existence of SCs is that they play a structural function, stabilizing the individual complexes [34,35] and/or serving as a platform for the efficient assembly of the complexes, with a special relevance for the biogenesis of mammalian CI [36-38].

Notably, the MRC structural organization, especially the stoichiometry, arrangements and stability of the SCs, may not be conserved in all eukaryotic species [39-42]. This is the case even within mammals, as human cells and tissues barely contain free CI, which is rather contained in SC I_1+III_2 and the respirasome [29,37]. In contrast, other mammalian mitochondria (from bovine, ovine, rat or mouse) contain larger amounts of CI in its free form, even if the majority is still mostly in the form of SCs [2,17,28,43-45]. The distribution of the MRC complexes between free complexes and SCs seems to differ even more in non-mammalian animal species. Several reptile species contain a very stable SC I+III_2 that lacks CIV [28], and in *Drosophila melanogaster* practically all of CI is free, SCs being almost completely absent [46,47]. However, comparative studies of MRC function in diverse animal species suggest that higher amounts and stability of the SCs do not correlate with increased respiratory activity/efficiency and/or reduced ROS production [28,47].

Here we show that SCs can be stably formed in *D. melanogaster* mitochondria upon mild perturbations of individual CIV, $CIII_2$ and CI biogenesis. This finding enabled us to test whether increased SC formation translated into enhanced respiration proficiency. However, MRC performance of fruit fly mitochondria did not change regardless of the presence or absence of SCs. These observations have led us to conclude that: 1) the efficiency in the assembly of the individual complexes is likely to be the main determinant

117 of SC formation and 2) these supramolecular complexes play a more relevant role in
118 maintaining the stability and/or supporting the biogenesis of the MRC than in promoting
119 catalysis.

RESULTS

D. melanogaster MRC organization does rely on SC formation under physiological conditions

To obtain a detailed characterization of MRC organization in *D. melanogaster,* we isolated mitochondria from wild-type adults and, after solubilization with digitonin, we performed Blue-Native Gel Electrophoresis (BNGE) followed by mass spectrometry analysis of the gel lanes, using 'Complexome Profiling (CP)' [48] and thus obtaining a profile of peptide intensities from most OXPHOS subunits along the electrophoresis lane (Figure 1A). This allowed us to unequivocally determine the identity of the main bands that can be visualized by Coomassie staining of BNGE gels (Figure 1B). The identity of the bands corresponding to complex I (CI) and complex IV (CIV) was also confirmed using specific in-gel activity (IGA) assays (Figure 1B). These analyses verified that *D. melanogaster* mitochondria contain extremely low amounts of high-molecular weight CI-containing SCs [46,47], using the same solubilization and electrophoresis conditions in which the SCs are readily detectable in mammalian cells and tissues [29,43,49]. As previously described [47], dimeric complex V (CV_2) is easily visualized by BNGE and present in similar amounts as monomeric CV in *D. melanogaster* mitochondrial membranes solubilized with digitonin (Figure 1A, B). This CV_2 species is not a strongly bound dimer, as it disappears when the samples are solubilized using a harsher detergent such as dodecylmaltoside (DDM) [47] (Figure 1C). Conversely, CI is mainly found as a free complex in the native gels irrespective of whether the mitochondria had been solubilized with digitonin or DDM (Figure 1A, B and C). The other minor CI-containing band corresponding to the fraction associated with $CIII_2$, accounts for about 3% of the total amounts of CI and $CIII_2$, according to label-free mass spectrometry quantifications in the CP analysis and densitometric quantifications of the CI-IGA signals (Figure 1A and Figure S1A). CIV activity is absent in this band both in digitonin- and DDM-solubilized samples (Figure 1B, C), whereas it is present in the bands that correspond to individual CIV and dimeric CIV (CIV_2) detected both in digitonin- and DDM-treated samples, as well as in SC III_2IV_1, which is present only in the digitonin-solubilized samples. This is different from mammalian mitochondria in which SC III_2IV_1 is present also in DDM-solubilized mitochondria, probably due to the tight binding of $CIII_2$ to CIV through COX7A2L/SCAF1 [4,29,50]. The latter does not have a homolog in *D. melanogaster* even though this species has three different COX7A isoforms (named COX7A, COX7AL and COX7AL2) that exhibit a tissue-specific expression pattern. CP analysis of *Drosophila*

mitochondria only detected COX7A (mammalian COX7A1 homolog) and COX7AL2 (mammalian COX7A2 homolog), whereas COX7AL, that is solely expressed in testis, was not found. Therefore, SC I_1III_2 can be considered the only stable SC species in physiological conditions in *D. melanogaster*, yet containing a minute fraction of the total CI and $CIII_2$.

Perturbations of CIV assembly result in increased formation of SC I_1III_2

COA8 is a CIV assembly factor the defects of which cause isolated mitochondrial CIV deficiency in human and mouse [51,52], as well as in *Drosophila melanogaster* [53,54]. Consistent with the role of Coa8 in CIV biogenesis, CP analysis of mitochondria from *Coa8* knockout (*Coa8*^{KO}) flies showed a clear decrease in fully assembled CIV and in all the CIV-containing species (Figure 2A, B) when compared to the corresponding wild-type (WT) individuals (Figure 1A and Figure 2B). Curiously, CP also showed that in the *Coa8*^{KO} mitochondria the amounts of SC I_1III_2 were noticeably increased (Figure 2A, B). In these samples, complexes I and III_2 build a stable SC species containing ~16% of the total amount of CI, as visualized by CI-IGA, as well as by western blot (WB) and immunodetection of specific CI and $CIII_2$ subunits after BNGE in DDM-solubilized mitochondria (Figure 2C, D, Figure S1A and S2A). We initially speculated that the ~5-fold increase of SC I_1III_2 formation could be linked to the release of III_2 from SC III_2IV_1 induced by the strong reduction in CIV amounts when Coa8 is absent.

To test this hypothesis, we modulated Coa8 expression via UAS/GAL4 system using RNAi driven by a 'mild' ubiquitous GAL4 driver (*da-gal4*). With this system, the *Coa8* mRNA levels were reduced to ~60% of the control (Figure 3A). However, these flies showed comparable levels of fully assembled CIV (Figure 3B, Figure S2B). Interestingly, in this case there was also an increased formation of SC I_1III_2 from ~3% in the control to ~10% in the mild *Coa8*^{RNAi} (Figure 3B, C, Figure S1B). Therefore, both strong and weak perturbations of CIV assembly produce an increased formation of CI-containing SCs in *D. melanogaster,* irrespective of whether they result in CIV deficiency or not.

Enhanced formation of SC I_1III_2 does not result in increased respiratory rates.

SC formation was proposed to serve as a means to favor electron transfer between the complexes and therefore increase the efficiency of CI-fueled respiration [1]. With this in mind, the complete *Coa8*^{KO} and mild *Coa8*^{RNAi} fly mitochondria, which show increased amounts of SC I_1III_2 compared to the WT controls, provide an excellent opportunity to test

188 this possibility. Oxygen consumption activities of fly homogenates in presence of different
189 substrates and inhibitors were analyzed by high-resolution respirometry (Figure 4A, B).
190 The significant decrease in CIV enzymatic activity in the *Coa8*^{KO} (Figure 4C) was not
191 reflected by reduced oxygen consumption (Figure 4A). This could be explained as a result
192 of a high CIV excess in fly mitochondria, in which the observed 60% reduction in CIV
193 enzyme activity is still above the threshold at which the CIV defect determines lower
194 respiratory rates [55,56]. In contrast, the mild reduction in *Coa8* mRNA levels did not result in
195 CIV enzymatic deficiency but produced a slight elevation in CI amounts and activity
196 (Figure S1B, Figure 4D), which could be related to the increased SC I_1III_2 formation.
197 However, the *Coa8-KD* mitochondria did not show any differences in respiration with either
198 CI-linked or CII-linked substrates. Also, the increased and stable interactions between
199 complexes I and III_2 in the Coa8 deficient models did not produce a preferential utilization
200 of electrons coming from CI, which would be the prediction if SC formation increased
201 electron transfer efficiency [13].
202
203 **Mild perturbation of $CIII_2$ biogenesis also enhances SC formation in *D. melanogaster***
204 To determine whether increased SC I_1III_2 formation was specific for CIV deficient flies, we
205 targeted $CIII_2$ by knocking down the expression of *Bcs1*. BCS1L, the human homolog, is
206 fundamental for a correct $CIII_2$ biogenesis, being responsible for the incorporation of the
207 catalytic subunit UQCRFS1 in the last steps of $CIII_2$ maturation [57,58]. To obtain a severe
208 $CIII_2$ defect in *D. melanogaster*, we crossed a 'strong' ubiquitous GAL4 driver (*act5c-gal4*)
209 line with a *UAS-Bcs1* RNAi responder line [59]. The knockdown efficiency was high, with a
210 ~75% decrease in *Bcs1* expression at the mRNA level (Figure 5A). In this model, *D.*
211 *melanogaster* development was severely impaired causing an arrest at the larval stage [59].
212 The strong *Bcs1*^{RNAi} caused also a significant decrease in fully assembled $CIII_2$ levels
213 (Figure 5B, C, Figure S2C) and in $CIII_2$ enzymatic activity of about 50% (Figure 5D).
214 Consistent with the observed $CIII_2$ deficiency, both the CI- and CII- linked respiration rates
215 were significantly decreased by around 40% (Figure 5E).
216 In contrast, less pronounced decreases in *Bcs1* expression (Figure 5F) by using the mild
217 *da-gal4* driver instead, did not produce a noticeable $CIII_2$ enzymatic defect (Figure 5I).
218 However, the mild *Bcs1-KD* mitochondria showed a very different pattern of CI distribution
219 than the controls (Figure 5G, H, Figure S1D), showing much higher levels of SC I_1III_2 as
220 well as the appearance of a new higher molecular weight band containing also CIV, as
221 revealed by WB and immunodetection analyses (Figure 5G, H), similarly to the

222 mammalian respirasome (SC $I_1III_2IV_1$). At the functional level, this was associated with a
223 ~1.5-fold increase in CI enzymatic activity (Figure 5I), which is proportional to the increase
224 in total CI amounts (Figure S1D), and in higher CI-linked respiration rates but only by ~1.2-
225 fold (Figure 5J). CII-linked respiration was the same in the mild *Bcs1*^{RNAi} samples as in the
226 controls. Therefore, the formation of respirasome-like SCs in these mitochondria did
227 neither increase the efficiency of electron transfer from CI nor determine a diversion of the
228 electronic routes giving preference to the SC-bound CI.
229
230 **Mild perturbation of CI biogenesis also leads to increased SC assembly**
231 To understand the effect of the strong and mild perturbations in CI biogenesis on MRC
232 organization in D. melanogaster, we employed a similar strategy as that for CIII (see
233 above). Crossing the strong ubiquitous *act5c-gal4* driver fly line with the *UAS-Ndufs4* RNAi
234 responder line, produced a decrease in *Ndufs4* mRNA expression of ~90% (Figure 6A).
235 Defects in *NDUFS4* are a major cause of CI deficiency-associated mitochondrial disease
236 in humans [60] and the mouse and *D. melanogaster* animal models display CI deficiency and
237 pathological phenotypes [61,62]. Accordingly, the strong reduction in Ndufs4 expression
238 observed in our models resulted in developmental arrest and a significant decrease in fully
239 assembled CI levels by ~40% (Figure 6B, C, Figure S1E) and in a proportional decrease in
240 NADH:CoQ oxidoreductase enzyme activity in the larvae (Figure 6D). BNGE analysis of
241 the strong *Ndufs4*^{RNAi} *D. melanogaster* mitochondria, revealed the presence of a CI
242 subassembly, containing the core Ndufs3 subunit (Figure 6C, Figure S2E) but lacking
243 NADH-dehydrogenase activity (Figure 6B). This is similar to what is observed in NDUFS4-
244 deficient human and mouse, which accumulate the so-called ~830 kDa intermediate
245 lacking the N-module and stabilized by the NDUFAF2 assembly factor [63-65]. In contrast,
246 CIV levels and enzyme activity were significantly increased by 1.5-fold in the strong
247 *Ndufs4-KD* (Figure 6C, D, Figure S2E). CI-linked respiration measured in isolated
248 mitochondria from these flies was significantly lower than in the controls, whereas the CII-
249 linked respiration was comparable to the control (Figure 6E). These observations are
250 compatible with the isolated CI defect displayed by the strong *Ndufs4-KD* flies.
251 Conversely, when *Ndufs4* mRNA expression was reduced to about half of the control
252 levels (Figure 6F), a milder defect in CI abundance (Figure S1F, Figure S2F), which did
253 not affect either NADH:CoQ oxidoreductase enzymatic activity or respiratory capacity was
254 observed (Figure 6G, H, I, J) in the adult flies. However, smaller amounts of the inactive
255 sub-CI were still detectable (Figure 6H). Interestingly enough, this milder perturbation of CI

256 biogenesis by reducing the amounts of Ndufs4 also produced an increase in the formation
257 of SC I_1III_2 (Figure 6G, H), without any changes in respiratory performance compared to
258 the controls (Figure 6J).
259
260
261
262

DISCUSSION

The first description of MRC SCs in the early 2000's led to opposite opinions on whether these were real and functionally relevant entities. On the one hand, researchers argued that the random collision model and diffusion of the individual MRC complexes was well established experimentally and the idea of the SCs did not fit with these observations. On the other hand, others considered that these SCs were real entities and therefore they must have a functional relevance, mainly as a means to enhance electron transfer between the individual complexes. Presently, the existence of the SCs is not debated anymore, especially after the determination of the high resolution structures by cryo-electron microscopy (EM), first of the mammalian respirasomes (reviewed in [66]), followed by that of other mammalian SCs [3,4], and of mitochondrial respiratory chain SCs from other eukaryotic species [39-42,67,68]. However, whether SCs provide any catalytical advantage to the MRC or not, is still being debated and opposing views continue to exist [18,69-72]. The recent resolution of MRC SCs from different eukaryotic species has revealed that the relative arrangement of the complexes within the SCs and the bridging subunits varies substantially depending on the species. Therefore, given the conservation of the structures of the individual complexes, one could argue that if SC formation was of capital importance for MRC function, the way the complexes interact should be strictly conserved as well. Importantly, neither in the mammalian respirasomes, nor in the mammalian and plant SC I_1III_2 there is any evidence of substrate channeling, as the CoQ binding sites in CI and $CIII_2$ are too far apart to allow for this phenomenon to happen [3,4,18,41]. This is in agreement with different sets of functional data indicating that CoQ is interchangeable between the CI-containing SCs and the rest of the MRC [24,25,29,37]. Therefore, this contrasts with the possible segmentation of the CoQ pool - one dedicated to the respirasome and the other to the $FADH_2$-linked enzymes – which has been proposed to take place as a consequence of respirasome formation [12-14]. A further element against the notion that SC formation is essential for mitochondrial function, is the fact that in normal conditions the MRC of *D. melanogaster* is predominantly organized based on individual complexes, as shown by us in this work and by others [46,47]. The *Drosophila* organization was justified by a tighter packing within the mitochondrial cristae and a higher concentration of the mobile electron transporters, as a way to compensate for the lack of SCs [47]. However, inter-species differences in MRC organization do not appear to be of great relevance to determine the level of functionality [28]. For example, disaggregation of CI from the SCs in *A. thaliana*, where there are normally present, did not affect plant viability [73]. Altogether, these

297 observations argue against the strict requirement of SC formation to maintain MRC
298 function.
299 The second main proposed role for SC is that of stabilizing and/or favoring the assembly of
300 the individual complexes, especially that of CI [37,38,74]. Very recently, the *D. melanogaster*
301 CI structure has been solved [75,76]. This has provided a structural explanation as to why this
302 complex is majorly found as an individual entity, which seems to be due to a more stable
303 association of the NDUFA11 subunit in the *D. melanogaster* complex [76]. Subunit
304 NDUFA11 stabilizes the transmembrane helix anchoring the lateral helix of subunit MT-
305 ND5, bridging the two parts of the membrane arm of CI. In other systems, $CIII_2$ and, thus,
306 SC formation seem to be important for stabilizing the interaction of NDUFA11 in the CI
307 membrane domain instead [3,5,41,77]. However, in this work we show that there are ways to
308 induce the formation of CI-containing SCs in fruit fly mitochondria where they normally do
309 not exist. For example, whereas a strong impairment of $CIII_2$ biogenesis resulted in $CIII_2$
310 deficiency, decreased respiration and equal amounts of assembled CI, a mild perturbation
311 of $CIII_2$ biogenesis did not result in any MRC deficiency but rather in increased CI total
312 amounts, mainly due to enhanced SC formation. Similarly, strong decreases in Ndufs4
313 expression resulted in low CI amounts and activity, but milder decreases did not affect CI
314 function although CI was redistributed into supramolecular species. In contrast, both the
315 complete KO and mild KD of *Coa8*, induced a significantly increased formation of CI-
316 containing SCs. Even though the *Coa8*^{KO} flies display a significant reduction in CIV
317 amounts and activity, the loss of COA8 is associated with milder phenotypes in humans,
318 mouse and flies compared with the lack or dysfunction of other CIV assembly factors
319 [51,52,54]. Therefore, we propose that a partial loss of CIV assembly also induces the
320 formation of SCs in *D. melanogaster*. These observations are in line with the idea that in
321 situations of suboptimal MRC complex biogenesis, formation of CI-containing SCs could
322 be a way to structurally stabilize the system and preserve its function [65,78]. In the context of
323 the cooperative assembly model, where partially assembled complexes get together
324 before completion forming SC precursors [38], one could envision that slower assembly
325 kinetics would increase the chance of interactions at early stages, letting SC assembly
326 occur in a stable way. Difference in the kinetics of CIV assembly have been observed
327 between human and mouse fibroblasts, which is slower in the human cells [79]. Therefore,
328 differences in assembly kinetics could also explain the observed different amounts and
329 stoichiometries of the MRC SCs in different organisms. This is an interesting open
330 question that will deserve further future investigation. In any case, this enhanced SC

formation did not translate in an increase in respiratory function nor in a change in substrate preference in any of the tested models. If CI-containing SC formation enhanced respiratory activity significantly, we should have had detected a noticeable increase in CI-linked respiration in all the models of mild perturbation of CIV, $CIII_2$ and CI. Although we did observe higher respiration with CI-linked substrates in the mild *Bcs1*-KD, this was even lower to the increase in CI enzymatic activity and total abundance.

Therefore, we conclude that the main role of SC formation is to provide structural stability to the MRC, principally for CI, rather than to enhance electron transfer between the complexes during respiration.

342

343 ## KEY RESOURCES TABLE

REAGENT or RESOURCE	SOURCE	IDENTIFIER
Antibodies		
Mouse monoclonal anti-NDUFS3	Abcam	Ab14711; RRID:AB_301429
Rabbit polyclonal anti-COXIV	Cell Signaling Technology	#4844; RRID:AB_2085427
Rabbit polyclonal anti-UQCR-C2	Dr. Edward Owusu-Ansah, Columbia University, NY	N/A
Rabbit polyclonal anti-SdhA	Dr. Edward Owusu-Ansah, Columbia University, NY	N/A
Chemicals, peptides, and recombinant proteins		
3,30-Diaminobenzidine tetrahydrochloride hydrate	Merck	D5637
6-Aminocaproic acid	Merck	A2504
Acetyl coenzyme A lithium salt	Merck	A2181
Antimycin A	Merck	A8674
BSA (fatty acid free)	Merck	A6003
Catalase from bovine liver	Merck	C9322
Coenzyme Q1	Merck	C7956
Cytochrome c from equine heart	Merck	C7752
D-Mannitol	Merck	M4125
DCIP (2,6-Dichloroindophenol Sodium Salt Hydrate)	Merck	D1878
Decylubiquinone	Merck	D7911
Digitonin, High Purity	Calbiochem	300410
DTNB (5,5′-Dithiobis(2-nitrobenzoic acid))	Merck	D218200
EDTA (Ethylenediaminetetraacetic acid disodium salt dihydrate)	Merck	E1644
EGTA (Ethylene glycol-bis(2-aminoethylether)-N,N,N′,N′-tetraacetic acid)	Merck	E3889
HEPES (N-(2-Hydroxyethyl)piperazine-N′-(2-ethanesulfonic acid), 4-(2-Hydroxyethyl)piperazine-1-ethanesulfonic acid)	Merck	H3375
KCN (Potassium cyanide)	Merck	31252
Magnesium chloride hexahydrate	Merck	M2670
Malonic acid	Merck	M1296
n-Dodecyl-beta-maltoside (DDM)	Merck	D4641
NADH (β-Nicotinamide adenine dinucleotide, reduced dipotassium salt)	Merck	N4505
NativePAGE™ Cathode Buffer Additive	Thermo Fisher Scientific	BN2002
NativePAGE™ Running Buffer	Thermo Fisher Scientific	BN2001
Nitrotetrazolium Blue chloride	Merck	N6876
Oligomycin from Streptomyces diastatochromogenes	Merck	O4876
Oxaloacetic acid	Merck	O4126
Phospho(enol)pyruvic acid monopotassium salt	Merck	860077
Potassium borohydride	Merck	438472

Potassium phosphate dibasic	Merck	P2222
Potassium phosphate monobasic	Merck	P5655
Rotenone	Merck	R8875
Sodium hydrosulphite	Merck	157953
Sodium succinate	Merck	S2378
Sucrose	Merck	S7903
TRIS base	Merck	T1503
Tween-20	Merck	P7949
Critical commercial assays		
GoScript® Reverse Transcriptase Kit	Promega	A5001
GoTaq® qPCR Master Mix	Promega	A6001
Experimental models: Organisms/strains		
D. melanogaster strain *act5c-gal4*	BDSC	4414
D. melanogaster strain *da-gal4*	BDSC	8641
D. melanogaster strain UAS-Ndufs4 RNAi	VDRC	101489
D. melanogaster strain UAS-Bcs1 RNAi	BDSC	51863
D. melanogaster strain UAS-Coa8 RNAi	VDRC	100605
D. melanogaster strain Coa8 KO	Wellgenetics Inc.	N/A
Oligonucleotides		
Bcs1-Fw-qPCR: CTGAATGTTGCGCCAGAG	Thermo Fisher Scientific	N/A
Bcs1-Rv-qPCR: GACGAATGCTGCGTCGAT	Thermo Fisher Scientific	N/A
Coa8-Fw-qPCR: CAATAAGCGCTTCTACGAGGA	Thermo Fisher Scientific	N/A
Coa8-Rv-qPCR: CCAGTTCTTGTCGAGGAACG	Thermo Fisher Scientific	N/A
Ndufs4-Fw-qPCR: AAGATCACCGTGCCGACTG	Thermo Fisher Scientific	N/A
Ndufs4-Rv-qPCR: GACAATGGGTCGCCGCTG	Thermo Fisher Scientific	N/A
Rp49-Fw-qPCR: ATCGGTTACGGATCGAACAA	Thermo Fisher Scientific	N/A
Rp49-Rv-qPCR: GACAATCTCCTTGCGCTTCT	Thermo Fisher Scientific	N/A
Software and algorithms		
CFX Manager 3.0	Bio-Rad	1845000
Excel 16.69.1	Microsoft	https://www.microsoft.com/en-us/microsoft-365/excel
Graphpad Prism 8	GraphPad Software	https://www.graphpad.com/scientific-software/prism/
Fiji v2.0.0-rc-69/1.52p	ImageJ	https://imagej.net/software/fiji/downloads
GelAnalyzer v19.1	GelAnalyzer	http://www.gelanalyzer.com
MaxQuant v1.6.10.43	[80]	https://www.maxquant.org/
Other		
NativePAGE 3-12% Bis-Tris Gels	Thermo Fisher Scientific	BN1001BOX

PVDF Transfer Membrane, 0.45 µm, 26.5 cm x 3.75 m	Thermo Fisher Scientific	88518
XCell SureLock™ Mini-Cell	Thermo Fisher Scientific	EI0001

METHOD DETAILS

Fly stocks and maintenance

Fly stocks were raised on standard cornmeal medium and kept at 23°C, 70% humidity on a 12:12 hours light/dark cycle. Strains used in this study were obtained from Bloomington Drosophila Stock Center (BDSC) and Vienna Drosophila Resource Center (VDRC). Genotypes used in this study were: *act5c-gal4* (BDSC 4414), *da-gal4* (BDSC 8641), *UAS-Ndufs4 RNAi* (VDRC 101489), *UAS-Bcs1 RNAi* (BDSC 51863), *UAS-Coa8 RNAi* (VDRC 100605). Control strains were obtained in each experiment by crossing the specific *gal4* driver line with the genetic background flies w^{1118}. *Coa8* KO flies were generated by Wellgenetics Inc. by using CRISPR/Cas9 technology, generating a 676bp deletion, from the -49th nucleotide relative to ATG to the -34th nucleotide relative to the stop codon of Coa8.

RNA isolation, reverse transcription, and qRT-PCR

Total RNA was extracted from 10 individuals for each genotype using TRIzol method (Thermo Fisher Scientific) according to the manufacturer's protocol. Reverse transcription was performed with the GoScript Reverse Transcriptase kit (Promega). qRT-PCRs were performed using GoTaq qPCR SYBR Green chemistry (Promega) and a Bio-Rad CFX 96 Touch System (Bio-Rad). The $2^{-\Delta\Delta}$Ct method was used to calculate the expression levels of the targets (*Bcs1, Ndufs4, Coa8*) using *Rp49* as endogenous control. The oligonucleotides used are listed in the Key Resource Table

Isolation of Mitochondria

Mitochondria from *D. melanogaster* larvae and adults were prepared by homogenization and differential centrifugation as described in [81]. Protein concentration of mitochondrial extracts was measured with the Bio-Rad protein assay, based on the Bradford method.

Blue-native polyacrylamide gel electrophoresis (BN-PAGE) and in-gel activity (IGA) assays

376 Isolated mitochondria were solubilized in 1.5M aminocaproic acid, 50 mM Bis-Tris/HCl pH
377 7.0. The samples were solubilized with 4 mg of digitonin (Calbiochem) or 4 mg n-dodecyl
378 β-D-maltoside (Sigma) per mg of protein. After 5 min of incubation on ice, samples were
379 centrifuged at 18,000 X *g* at 4 °C for 30 min. The supernatant was collected and
380 resuspended with Sample Buffer (750 mM aminocaproic acid, 50 mM Bis-Tris/HCl pH 7.0,
381 0.5 mM EDTA and 5% Serva Blue G). Native samples were separated using NativePAGE
382 3-12% Bis-Tris gels (Thermo Fisher Scientific) according to the manufacturer's protocol.
383 For Coomassie staining, gels were stained with Coomassie R 250 for 20 minutes and
384 destained/fixed using 20% methanol, 7% acetic acid. For in-gel activity assays, gels were
385 stained with the following solutions: complex II (succinate dehydrogenase): 5 mM Tris–HCl
386 pH 7.4, 0.2 mM phenazine methosulfate (Sigma), 20 mM succinate, and 1 mg/ml
387 nitrotetrazolium blue chloride; Complex IV (cytochrome *c* oxidase): 50 mM potassium
388 phosphate pH 7.4, 1 mg/ml 3′,3′-diaminobenzidine tetrahydrochloride hydrate (Sigma), 24
389 units/ml catalase from bovine liver (Sigma), 1 mg/ml cytochrome *c* from equine heart
390 (Sigma), and 75 mg/ml sucrose [82].
391
392 **Complexome profiling**
393 Mitochondria from *D. melanogaster* were analyzed by complexome profiling [83]. Isolated
394 mitochondria (0.2 mg) were solubilized with 6 g digitonin/g protein in 50 mM NaCl, 5 mM 6-
395 aminohexanoic acid, 1 mM EDTA, 50 mM imidazole/HCl, pH 7.0. After centrifugation at
396 22,000 X *g* for 20 min at 4°C, the supernatant was supplemented with Coomassie brilliant
397 blue G250 and proteins were separated by 4-16% gradient BN-PAGE. Digitonin-
398 solubilized mitochondrial proteins from bovine heart were loaded as molecular mass
399 standards. Gel lanes were cut into 60 slices, transferred to a 96-well filter microtiter plate
400 (Millipore), and destained in 50% (v/v) methanol, 50 mM ammonium bicarbonate. After
401 destaining, in-gel digestion with trypsin was performed. Tryptic peptides were separated by
402 liquid chromatography and analyzed by tandem mass spectrometry (LC-MS/MS) in a Q-
403 Exactive 2.0 Orbitrap Mass Spectrometer (2.8 SP1) equipped with an Easy nLC1000
404 nano-flow ultra-high-pressure liquid chromatography system (Thermo Fisher Scientific) at
405 the front end. Thermo Scientific Xcalibur 3.1 Software Package was used for data
406 recording. MS RAW data files were analyzed using MaxQuant (version 1.5.0.25). The
407 extracted spectra were matched against the *Drosophila melanogaster* Uniprot Reference
408 Sequence database (release 2020_04). Database searches were done with 20 ppm match
409 tolerances. Trypsin was selected as the protease with two missed cleavages allowed.

410 Dynamic modifications included N-terminal acetylation and oxidation of methionine.
411 Cysteine carbamidomethylation was set as a fixed modification. Keratins, and trypsin were
412 removed from the list. The abundance of each protein was determined by label-free
413 quantification using the composite intensity based absolute quantification (iBAQ) values
414 determined by MaxQuant analysis and was corrected for loading and MS sensitivity
415 variations between samples based on the total iBAQ value for all detected complex V
416 subunits. Gel migration profiles were created for each protein and normalized to the
417 maximum abundance. Profiles of the identified mitochondrial proteins were hierarchically
418 clustered by distance measures based on Pearson correlation coefficient (uncentered) and
419 the average linkage method using the NOVA software package v0.5 [84]. The visualization
420 and analysis of the heatmaps representing the normalized abundance in each gel slice by
421 a three-color code gradient (black/yellow/red) were done using Microsoft Excel 2019 and
422 Graph Pad Prism 8.4.3. The mass calibration for the BN-PAGE gels was performed as
423 previously described [85]. Membrane proteins were calibrated using the well-known
424 molecular masses of respiratory chain complexes and supercomplexes from bovine heart
425 mitochondria. The soluble proteins were, however, calibrated using the following set of
426 *Drosophila* proteins: ATPB (51 kDa), malate dehydrogenase (72 kDa, dimer), citrate
427 synthase (100 kDa, dimer), ETFA/B (122, heterodimer), heat shock protein 60 (410 kDa,
428 heptamer), ALDH7A1 (675 kDa, dodecamer).
429
430 **Western blot and immunodetection**
431 BN-PAGE gels were transferred to PVDF membranes in Dunn carbonate buffer (10 mM
432 $NaHCO_3$, 3 mM Na_2CO_3) applying a constant current of 300 mA at 4°C for 1 hour using a
433 Mini Trans-Blot® Cell (Bio-Rad). For the immunodetection of specific protein targets,
434 blotted PVDF membranes were blocked in 5% skimmed milk in PBS-T (0.1% Tween-20) at
435 room temperature for 1 hour and then incubated overnight with primary antibodies diluted
436 in 3% BSA in PBS-T overnight at 4°C. PVDF membranes were washed three times with
437 PBS-T for 10 minutes, incubated with the secondary HRP- conjugated antibody for 1 hour
438 at room temperature and washed three times with PBS-T for 10 minutes.
439 Chemiluminescent signals were recorded using an Alliance Mini HD9 (UVITEC).
440 Antibodies used are listed in the Key Resource Table. The primary antibodies against *D.*
441 *melanogaster* UQCR-C2 and SdhA were a kind gift of Dr. Edward Owusu-Ansah
442 (Columbia University, NY).
443

444 **High-resolution respirometry**

445 To measure oxygen consumption individuals were homogenized on ice in respiration
446 buffer (120 mM sucrose, 50 mM KCl, 20 mM Tris-HCl, 4 mM KH_2PO_4, 2 mM $MgCl_2$, 1 mM
447 EGTA, 1% fatty acid-free BSA, pH 7.2). Homogenates were loaded in the chamber of an
448 O2k-HRR (High Resolution Respirometer, Oroboros Instruments) Complex I-linked
449 respiration was measured at saturating concentrations of malate (2 mM), glutamate (10
450 mM), proline (10 mM) and ADP (2.5 mM). Afterwards, complex II-linked respiration was
451 assessed using 10 mM succinate to the reaction after inhibition of complex I with rotenone
452 (1.25 μM).

453

454 **Analysis of MRC enzymatic activities**

455 The activities of mitochondrial respiratory chain complexes and citrate synthase (CS) were
456 measured using kinetic spectrophotometric assays as described [81].

457

458 **Statistical analysis**

459 Statistical analysis was performed with GraphPad Prism Software, version 8.2.1. Statistical
460 tests and significance are described in the figure captions.

461

462 **Data availability**

463 Complexome profiling data will be deposited in the ComplexomE profiling DAta Resource
464 (CEDAR) repository [86]. Data will be available upon manuscript acceptance.

465

ACKNOWLEDGEMENTS

We are grateful to Prof. Rodolfo Costa (CNR institute of Neuroscience, Padova, Italy) for providing the Coa8 KO and Bcs1 and Ndufs4 RNAi lines, Dr. Edward Owusu-Ansah (Columbia University, NY) for sharing the antibodies against *D. melanogaster* UQCR-C2 and SdhA and to Prof. Paolo Bernardi (Dept. of Biomedical Sciences, University of Padova) for critically reading the manuscript.

This research was funded by Fondazione Telethon-Cariplo Alliance GJC21014 (to E.F.-V.), Telethon Foundation GGP19007 (to M.Z.) and GGP20013 (to C.V.), AFM-Telethon 23706 (to C.V.), Department of Biomedical Sciences (University of Padova) FERN_FAR22_01 (to E.F.-V.) and SID2022- VISC_BIRD2222_01 (to C.V.), and Associazione Luigi Comini Onlus (MitoFight2, to M.Z. and C.V.).

AUTHOR CONTRIBUTIONS

Conceptualization, M.B., M.Z. and E.F.-V.; Methodology, M.B., A.C.-O., S.A. and E.F.-V.; Formal analysis, M.B., A.C.-O., S.A. and E.F.-V.; Investigation, M.B. and A.C.-O.; Data Curation, M.B., A.C.-O., S.A. and E.F.-V.; Writing-Original Draft, M.B. and E.F.-V.; Writing-Review & Editing, M.B., A.C.-O., S.A., M.Z. and E.F.-V.; Visualization, M.B. and E.F.-V.; Supervision, S.A., M.Z., C.V. and E.F-V.; Project Administration, M.B., M.Z., C.V. and E.F.-V.; Funding Acquisition, M.Z., C.V. and E.F.-V.

CONFLICT OF INTEREST

The authors declare no competing interests.

491 **REFERENCES**

492 1. Schagger, H., and Pfeiffer, K. (2000). Supercomplexes in the respiratory chains of
493 yeast and mammalian mitochondria. The EMBO journal *19*, 1777-1783.
494 10.1093/emboj/19.8.1777.
495 2. Schagger, H., and Pfeiffer, K. (2001). The ratio of oxidative phosphorylation
496 complexes I-V in bovine heart mitochondria and the composition of respiratory
497 chain supercomplexes. J Biol Chem *276*, 37861-37867.
498 3. Letts, J.A., Fiedorczuk, K., Degliesposti, G., Skehel, M., and Sazanov, L.A. (2019).
499 Structures of Respiratory Supercomplex I+III2 Reveal Functional and
500 Conformational Crosstalk. Molecular cell *75*, 1131-1146 e1136.
501 10.1016/j.molcel.2019.07.022.
502 4. Vercellino, I., and Sazanov, L.A. (2021). Structure and assembly of the mammalian
503 mitochondrial supercomplex CIII2CIV. Nature *598*, 364-367. 10.1038/s41586-021-
504 03927-z.
505 5. Letts, J.A., Fiedorczuk, K., and Sazanov, L.A. (2016). The architecture of
506 respiratory supercomplexes. Nature *537*, 644-648. 10.1038/nature19774.
507 6. Gu, J., Wu, M., Guo, R., Yan, K., Lei, J., Gao, N., and Yang, M. (2016). The
508 architecture of the mammalian respirasome. Nature *537*, 639-643.
509 10.1038/nature19359.
510 7. Sousa, J.S., Mills, D.J., Vonck, J., and Kuhlbrandt, W. (2016). Functional
511 asymmetry and electron flow in the bovine respirasome. Elife *5*.
512 10.7554/eLife.21290.
513 8. Wu, M., Gu, J., Guo, R., Huang, Y., and Yang, M. (2016). Structure of Mammalian
514 Respiratory Supercomplex I1III2IV1. Cell *167*, 1598-1609 e1510.
515 10.1016/j.cell.2016.11.012.
516 9. Guo, R., Zong, S., Wu, M., Gu, J., and Yang, M. (2017). Architecture of Human
517 Mitochondrial Respiratory Megacomplex I2III2IV2. Cell *170*, 1247-1257 e1212.
518 10.1016/j.cell.2017.07.050.
519 10. Bianchi, C., Genova, M.L., Parenti Castelli, G., and Lenaz, G. (2004). The
520 mitochondrial respiratory chain is partially organized in a supercomplex assembly:
521 kinetic evidence using flux control analysis. J Biol Chem *279*, 36562-36569.
522 11. Lenaz, G., and Genova, M.L. (2007). Kinetics of integrated electron transfer in the
523 mitochondrial respiratory chain: random collisions vs. solid state electron

524 channeling. Am J Physiol Cell Physiol *292*, C1221-1239.
525 10.1152/ajpcell.00263.2006.
526 12. Lenaz, G., and Genova, M.L. (2009). Mobility and function of coenzyme Q
527 (ubiquinone) in the mitochondrial respiratory chain. Biochim Biophys Acta *1787*,
528 563-573. 10.1016/j.bbabio.2009.02.019.
529 13. Lapuente-Brun, E., Moreno-Loshuertos, R., Acin-Perez, R., Latorre-Pellicer, A.,
530 Colas, C., Balsa, E., Perales-Clemente, E., Quiros, P.M., Calvo, E., Rodriguez-
531 Hernandez, M.A., et al. (2013). Supercomplex assembly determines electron flux in
532 the mitochondrial electron transport chain. Science *340*, 1567-1570.
533 10.1126/science.1230381.
534 14. Calvo, E., Cogliati, S., Hernansanz-Agustin, P., Loureiro-Lopez, M., Guaras, A.,
535 Casuso, R.A., Garcia-Marques, F., Acin-Perez, R., Marti-Mateos, Y., Silla-Castro,
536 J.C., et al. (2020). Functional role of respiratory supercomplexes in mice: SCAF1
537 relevance and segmentation of the Qpool. Sci Adv *6*, eaba7509.
538 10.1126/sciadv.aba7509.
539 15. Garcia-Poyatos, C., Cogliati, S., Calvo, E., Hernansanz-Agustin, P., Lagarrigue, S.,
540 Magni, R., Botos, M., Langa, X., Amati, F., Vazquez, J., et al. (2020). Scaf1
541 promotes respiratory supercomplexes and metabolic efficiency in zebrafish. EMBO
542 Rep *21*, e50287. 10.15252/embr.202050287.
543 16. Maranzana, E., Barbero, G., Falasca, A.I., Lenaz, G., and Genova, M.L. (2013).
544 Mitochondrial respiratory supercomplex association limits production of reactive
545 oxygen species from complex I. Antioxid Redox Signal *19*, 1469-1480.
546 10.1089/ars.2012.4845.
547 17. Lopez-Fabuel, I., Le Douce, J., Logan, A., James, A.M., Bonvento, G., Murphy,
548 M.P., Almeida, A., and Bolanos, J.P. (2016). Complex I assembly into
549 supercomplexes determines differential mitochondrial ROS production in neurons
550 and astrocytes. Proceedings of the National Academy of Sciences of the United
551 States of America *113*, 13063-13068. 10.1073/pnas.1613701113.
552 18. Hirst, J. (2018). Open questions: respiratory chain supercomplexes-why are they
553 there and what do they do? BMC Biol *16*, 111. 10.1186/s12915-018-0577-5.
554 19. Green, D.E., and Tzagoloff, A. (1966). The mitochondrial electron transfer chain.
555 Arch Biochem Biophys *116*, 293-304. 10.1016/0003-9861(66)90036-1.

556 20. Kröger, A., and Klingenberg, M. (1973). Further evidence for the pool function of
557 ubiquinone as derived from the inhibition of the electron transport by antimycin. Eur
558 J Biochem *39*, 313-323. 10.1111/j.1432-1033.1973.tb03129.x.
559 21. Kröger, A., and Klingenberg, M. (1973). The kinetics of the redox reactions of
560 ubiquinone related to the electron-transport activity in the respiratory chain. Eur J
561 Biochem *34*, 358-368. 10.1111/j.1432-1033.1973.tb02767.x.
562 22. Hackenbrock, C.R., Chazotte, B., and Gupte, S.S. (1986). The random collision
563 model and a critical assessment of diffusion and collision in mitochondrial electron
564 transport. Journal of bioenergetics and biomembranes *18*, 331-368.
565 23. Chazotte, B., and Hackenbrock, C.R. (1988). The multicollisional, obstructed, long-
566 range diffusional nature of mitochondrial electron transport. J Biol Chem *263*,
567 14359-14367.
568 24. Blaza, J.N., Serreli, R., Jones, A.J., Mohammed, K., and Hirst, J. (2014). Kinetic
569 evidence against partitioning of the ubiquinone pool and the catalytic relevance of
570 respiratory-chain supercomplexes. Proceedings of the National Academy of
571 Sciences of the United States of America *111*, 15735-15740.
572 10.1073/pnas.1413855111.
573 25. Fedor, J.G., and Hirst, J. (2018). Mitochondrial Supercomplexes Do Not Enhance
574 Catalysis by Quinone Channeling. Cell Metab *28*, 525-531 e524.
575 10.1016/j.cmet.2018.05.024.
576 26. Mourier, A., Matic, S., Ruzzenente, B., Larsson, N.G., and Milenkovic, D. (2014).
577 The respiratory chain supercomplex organization is independent of COX7a2l
578 isoforms. Cell Metab *20*, 1069-1075. 10.1016/j.cmet.2014.11.005.
579 27. Lobo-Jarne, T., Nyvltova, E., Perez-Perez, R., Timon-Gomez, A., Molinie, T., Choi,
580 A., Mourier, A., Fontanesi, F., Ugalde, C., and Barrientos, A. (2018). Human
581 COX7A2L Regulates Complex III Biogenesis and Promotes Supercomplex
582 Organization Remodeling without Affecting Mitochondrial Bioenergetics. Cell reports
583 *25*, 1786-1799 e1784. 10.1016/j.celrep.2018.10.058.
584 28. Bundgaard, A., James, A.M., Harbour, M.E., Murphy, M.P., and Fago, A. (2020).
585 Stable mitochondrial CICIII2 supercomplex interactions in reptiles versus
586 homeothermic vertebrates. The Journal of experimental biology *223*, jeb223776.
587 10.1242/jeb.223776.
588 29. Fernandez-Vizarra, E., Lopez-Calcerrada, S., Sierra-Magro, A., Perez-Perez, R.,
589 Formosa, L.E., Hock, D.H., Illescas, M., Penas, A., Brischigliaro, M., Ding, S., et al.

590 (2022). Two independent respiratory chains adapt OXPHOS performance to
591 glycolytic switch. Cell Metab *34*, 1792-1808. 10.1016/j.cmet.2022.09.005.
592 30. Berndtsson, J., Aufschnaiter, A., Rathore, S., Marin-Buera, L., Dawitz, H., Diessl, J.,
593 Kohler, V., Barrientos, A., Buttner, S., Fontanesi, F., and Ott, M. (2020). Respiratory
594 supercomplexes enhance electron transport by decreasing cytochrome c diffusion
595 distance. EMBO Rep *21*, e51015. 10.15252/embr.202051015.
596 31. Stuchebrukhov, A., Schafer, J., Berg, J., and Brzezinski, P. (2020). Kinetic
597 advantage of forming respiratory supercomplexes. Biochim Biophys Acta Bioenerg
598 *1861*, 148193. 10.1016/j.bbabio.2020.148193.
599 32. Trouillard, M., Meunier, B., and Rappaport, F. (2011). Questioning the functional
600 relevance of mitochondrial supercomplexes by time-resolved analysis of the
601 respiratory chain. Proceedings of the National Academy of Sciences of the United
602 States of America *108*, E1027-1034. 10.1073/pnas.1109510108.
603 33. Nesci, S., and Lenaz, G. (2021). The mitochondrial energy conversion involves
604 cytochrome c diffusion into the respiratory supercomplexes. Biochim Biophys Acta
605 Bioenerg *1862*, 148394. 10.1016/j.bbabio.2021.148394.
606 34. Acin-Perez, R., Bayona-Bafaluy, M.P., Fernandez-Silva, P., Moreno-Loshuertos, R.,
607 Perez-Martos, A., Bruno, C., Moraes, C.T., and Enriquez, J.A. (2004). Respiratory
608 Complex III Is Required to Maintain Complex I in Mammalian Mitochondria.
609 Molecular cell *13*, 805-815. 10.1016/s1097-2765(04)00124-8.
610 35. Diaz, F., Fukui, H., Garcia, S., and Moraes, C.T. (2006). Cytochrome c oxidase is
611 required for the assembly/stability of respiratory complex I in mouse fibroblasts.
612 Molecular and Cellular Biology *26*, 4872-4881. 10.1128/Mcb.01767-05.
613 36. Moreno-Lastres, D., Fontanesi, F., Garcia-Consuegra, I., Martin, M.A., Arenas, J.,
614 Barrientos, A., and Ugalde, C. (2012). Mitochondrial complex I plays an essential
615 role in human respirasome assembly. Cell Metab *15*, 324-335. S1550-
616 4131(12)00022-8 [pii]
617 10.1016/j.cmet.2012.01.015.
618 37. Protasoni, M., Perez-Perez, R., Lobo-Jarne, T., Harbour, M.E., Ding, S., Penas, A.,
619 Diaz, F., Moraes, C.T., Fearnley, I.M., Zeviani, M., et al. (2020). Respiratory
620 supercomplexes act as a platform for complex III-mediated maturation of human
621 mitochondrial complexes I and IV. The EMBO journal *39*, e102817.
622 10.15252/embj.2019102817.

623 38. Fernandez-Vizarra, E., and Ugalde, C. (2022). Cooperative assembly of the
624 mitochondrial respiratory chain. Trends Biochem Sci *47*, 999-1008.
625 10.1016/j.tibs.2022.07.005.
626 39. Maldonado, M., Guo, F., and Letts, J.A. (2021). Atomic structures of respiratory
627 complex III2, complex IV, and supercomplex III2-IV from vascular plants. Elife *10*,
628 e62047. 10.7554/eLife.62047.
629 40. Zhou, L., Maldonado, M., Padavannil, A., Guo, F., and Letts, J.A. (2022). Structures
630 of Tetrahymena's respiratory chain reveal the diversity of eukaryotic core
631 metabolism. Science *376*, 831-839. 10.1126/science.abn7747.
632 41. Maldonado, M., Fan, Z., Abe, K.M., and Letts, J.A. (2023). Plant-specific features of
633 respiratory supercomplex I + III(2) from Vigna radiata. Nat Plants *9*, 157-168.
634 10.1038/s41477-022-01306-8.
635 42. Klusch, N., Dreimann, M., Senkler, J., Rugen, N., Kuhlbrandt, W., and Braun, H.P.
636 (2023). Cryo-EM structure of the respiratory I + III(2) supercomplex from
637 Arabidopsis thaliana at 2 A resolution. Nat Plants *9*, 142-156. 10.1038/s41477-022-
638 01308-6.
639 43. Acin-Perez, R., Fernandez-Silva, P., Peleato, M.L., Perez-Martos, A., and Enriquez,
640 J.A. (2008). Respiratory active mitochondrial supercomplexes. Molecular cell *32*,
641 529-539. 10.1016/j.molcel.2008.10.021.
642 44. Letts, J.A., and Sazanov, L.A. (2017). Clarifying the supercomplex: the higher-order
643 organization of the mitochondrial electron transport chain. Nat Struct Mol Biol *24*,
644 800-808. 10.1038/nsmb.3460.
645 45. Davies, K.M., Blum, T.B., and Kuhlbrandt, W. (2018). Conserved in situ
646 arrangement of complex I and III2 in mitochondrial respiratory chain
647 supercomplexes of mammals, yeast, and plants. Proceedings of the National
648 Academy of Sciences of the United States of America *115*, 3024-3029.
649 10.1073/pnas.1720702115.
650 46. Garcia, C.J., Khajeh, J., Coulanges, E., Chen, E.I., and Owusu-Ansah, E. (2017).
651 Regulation of Mitochondrial Complex I Biogenesis in Drosophila Flight Muscles. Cell
652 reports *20*, 264-278. 10.1016/j.celrep.2017.06.015.
653 47. Shimada, S., Oosaki, M., Takahashi, R., Uene, S., Yanagisawa, S., Tsukihara, T.,
654 and Shinzawa-Itoh, K. (2018). A unique respiratory adaptation in Drosophila
655 independent of supercomplex formation. Biochim Biophys Acta Bioenerg *1859*, 154-
656 163. 10.1016/j.bbabio.2017.11.007.

657 48. Cabrera-Orefice, A., Potter, A., Evers, F., Hevler, J.F., and Guerrero-Castillo, S.
658 (2022). Complexome Profiling-Exploring Mitochondrial Protein Complexes in Health
659 and Disease. Front Cell Dev Biol *9*, 796128. 10.3389/fcell.2021.796128.
660 49. Wittig, I., Braun, H.P., and Schagger, H. (2006). Blue native PAGE. Nat Protoc *1*,
661 418-428.
662 50. Perales-Clemente, E., Fernandez-Vizarra, E., Acin-Perez, R., Movilla, N., Bayona-
663 Bafaluy, M.P., Moreno-Loshuertos, R., Perez-Martos, A., Fernandez-Silva, P., and
664 Enriquez, J.A. (2010). Five entry points of the mitochondrially encoded subunits in
665 Mammalian complex I assembly. Mol Cell Biol *30*, 3038-3047. MCB.00025-10 [pii]
666 10.1128/MCB.00025-10.
667 51. Melchionda, L., Haack, T.B., Hardy, S., Abbink, T.E., Fernandez-Vizarra, E.,
668 Lamantea, E., Marchet, S., Morandi, L., Moggio, M., Carrozzo, R., et al. (2014).
669 Mutations in APOPT1, Encoding a Mitochondrial Protein, Cause Cavitating
670 Leukoencephalopathy with Cytochrome c Oxidase Deficiency. Am J Hum Genet *95*,
671 315-325. 10.1016/j.ajhg.2014.08.003.
672 52. Signes, A., Cerutti, R., Dickson, A.S., Beninca, C., Hinchy, E.C., Ghezzi, D.,
673 Carrozzo, R., Bertini, E., Murphy, M.P., Nathan, J.A., et al. (2019). APOPT1/COA8
674 assists COX assembly and is oppositely regulated by UPS and ROS. EMBO
675 molecular medicine *11*. 10.15252/emmm.201809582.
676 53. Brischigliaro, M., Corra, S., Tregnago, C., Fernandez-Vizarra, E., Zeviani, M.,
677 Costa, R., and De Pitta, C. (2019). Knockdown of APOPT1/COA8 Causes
678 Cytochrome c Oxidase Deficiency, Neuromuscular Impairment, and Reduced
679 Resistance to Oxidative Stress in Drosophila melanogaster. Front Physiol *10*, 1143.
680 10.3389/fphys.2019.01143.
681 54. Brischigliaro, M., Badocco, D., Costa, R., Viscomi, C., Zeviani, M., Pastore, P., and
682 Fernandez-Vizarra, E. (2022). Mitochondrial Cytochrome c Oxidase Defects Alter
683 Cellular Homeostasis of Transition Metals. Front Cell Dev Biol *10*, 892069.
684 10.3389/fcell.2022.892069.
685 55. Villani, G., Greco, M., Papa, S., and Attardi, G. (1998). Low reserve of cytochrome c
686 oxidase capacity in vivo in the respiratory chain of a variety of human cell types. J
687 Biol Chem *273*, 31829-31836. 10.1074/jbc.273.48.31829.
688 56. Villani, G., and Attardi, G. (2000). In vivo control of respiration by cytochrome c
689 oxidase in human cells. Free Radic Biol Med *29*, 202-210.

690 57. Fernandez-Vizarra, E., Bugiani, M., Goffrini, P., Carrara, F., Farina, L., Procopio, E.,
691 Donati, A., Uziel, G., Ferrero, I., and Zeviani, M. (2007). Impaired complex III
692 assembly associated with BCS1L gene mutations in isolated mitochondrial
693 encephalopathy. Hum Mol Genet *16*, 1241-1252. 10.1093/hmg/ddm072.
694 58. Fernandez-Vizarra, E., and Zeviani, M. (2018). Mitochondrial complex III Rieske Fe-
695 S protein processing and assembly. Cell cycle *17*, 681-687.
696 10.1080/15384101.2017.1417707.
697 59. Brischigliaro, M., Frigo, E., Corra, S., De Pitta, C., Szabo, I., Zeviani, M., and Costa,
698 R. (2021). Modelling of BCS1L-related human mitochondrial disease in Drosophila
699 melanogaster. J Mol Med (Berl) *99*, 1471-1485. 10.1007/s00109-021-02110-1.
700 60. Ortigoza-Escobar, J.D., Oyarzabal, A., Montero, R., Artuch, R., Jou, C., Jimenez,
701 C., Gort, L., Briones, P., Muchart, J., Lopez-Gallardo, E., et al. (2016). Ndufs4
702 related Leigh syndrome: A case report and review of the literature. Mitochondrion
703 *28*, 73-78. 10.1016/j.mito.2016.04.001.
704 61. Kruse, S.E., Watt, W.C., Marcinek, D.J., Kapur, R.P., Schenkman, K.A., and
705 Palmiter, R.D. (2008). Mice with mitochondrial complex I deficiency develop a fatal
706 encephalomyopathy. Cell Metab *7*, 312-320. 10.1016/j.cmet.2008.02.004.
707 62. Foriel, S., Beyrath, J., Eidhof, I., Rodenburg, R.J., Schenck, A., and Smeitink,
708 J.A.M. (2018). Feeding difficulties, a key feature of the Drosophila NDUFS4
709 mitochondrial disease model. Dis Model Mech *11*. 10.1242/dmm.032482.
710 63. Vogel, R.O., van den Brand, M.A., Rodenburg, R.J., van den Heuvel, L.P.,
711 Tsuneoka, M., Smeitink, J.A., and Nijtmans, L.G. (2007). Investigation of the
712 complex I assembly chaperones B17.2L and NDUFAF1 in a cohort of CI deficient
713 patients. Mol Genet Metab *91*, 176-182. 10.1016/j.ymgme.2007.02.007.
714 64. Assouline, Z., Jambou, M., Rio, M., Bole-Feysot, C., de Lonlay, P., Barnerias, C.,
715 Desguerre, I., Bonnemains, C., Guillermet, C., Steffann, J., et al. (2012). A constant
716 and similar assembly defect of mitochondrial respiratory chain complex I allows
717 rapid identification of NDUFS4 mutations in patients with Leigh syndrome. Biochim
718 Biophys Acta *1822*, 1062-1069. 10.1016/j.bbadis.2012.01.013.
719 65. Calvaruso, M.A., Willems, P., van den Brand, M., Valsecchi, F., Kruse, S., Palmiter,
720 R., Smeitink, J., and Nijtmans, L. (2012). Mitochondrial complex III stabilizes
721 complex I in the absence of NDUFS4 to provide partial activity. Human molecular
722 genetics *21*, 115-120. 10.1093/hmg/ddr446.

723 66. Caruana, N.J., and Stroud, D.A. (2020). The road to the structure of the
724 mitochondrial respiratory chain supercomplex. Biochemical Society transactions *48*,
725 621-629. 10.1042/BST20190930.
726 67. Rathore, S., Berndtsson, J., Marin-Buera, L., Conrad, J., Carroni, M., Brzezinski, P.,
727 and Ott, M. (2019). Cryo-EM structure of the yeast respiratory supercomplex. Nat
728 Struct Mol Biol *26*, 50-57. 10.1038/s41594-018-0169-7.
729 68. Hartley, A.M., Lukoyanova, N., Zhang, Y., Cabrera-Orefice, A., Arnold, S., Meunier,
730 B., Pinotsis, N., and Marechal, A. (2019). Structure of yeast cytochrome c oxidase
731 in a supercomplex with cytochrome bc1. Nat Struct Mol Biol *26*, 78-83.
732 10.1038/s41594-018-0172-z.
733 69. Milenkovic, D., Blaza, J.N., Larsson, N.G., and Hirst, J. (2017). The Enigma of the
734 Respiratory Chain Supercomplex. Cell Metab *25*, 765-776.
735 10.1016/j.cmet.2017.03.009.
736 70. Hernansanz-Agustin, P., and Enriquez, J.A. (2021). Functional segmentation of
737 CoQ and cyt c pools by respiratory complex superassembly. Free Radic Biol Med
738 *167*, 232-242. 10.1016/j.freeradbiomed.2021.03.010.
739 71. Cogliati, S., Cabrera-Alarcon, J.L., and Enriquez, J.A. (2021). Regulation and
740 functional role of the electron transport chain supercomplexes. Biochemical Society
741 transactions *49*, 2655-2668. 10.1042/BST20210460.
742 72. Vercellino, I., and Sazanov, L.A. (2022). The assembly, regulation and function of
743 the mitochondrial respiratory chain. Nature reviews. Molecular cell biology *23*, 141-
744 161. 10.1038/s41580-021-00415-0.
745 73. Rohricht, H., Przybyla-Toscano, J., Forner, J., Boussardon, C., Keech, O., Rouhier,
746 N., and Meyer, E.H. (2023). Mitochondrial ferredoxin-like is essential for forming
747 complex I-containing supercomplexes in Arabidopsis. Plant Physiol.
748 10.1093/plphys/kiad040.
749 74. Lobo-Jarne, T., and Ugalde, C. (2018). Respiratory chain supercomplexes:
750 Structures, function and biogenesis. Semin Cell Dev Biol *76*, 179-190.
751 10.1016/j.semcdb.2017.07.021.
752 75. Agip, A.A., Chung, I., Sanchez-Martinez, A., Whitworth, A.J., and Hirst, J. (2023).
753 Cryo-EM structures of mitochondrial respiratory complex I from Drosophila
754 melanogaster. Elife *12*. 10.7554/eLife.84424.

755 76. Padavannil, A., Murari, A., Rhooms, S.-K., Owusu-Ansah, E., and Letts, J.A. (2022).
756 Resting mitochondrial complex I from Drosophila melanogaster adopts
757 a helix-locked state. bioRxiv, 2022.2011.2001.514701. 10.1101/2022.11.01.514701.
758 77. Padavannil, A., Ayala-Hernandez, M.G., Castellanos-Silva, E.A., and Letts, J.A.
759 (2022). The Mysterious Multitude: Structural Perspective on the Accessory Subunits
760 of Respiratory Complex I. Front Mol Biosci *8*, 798353. 10.3389/fmolb.2021.798353.
761 78. Tropeano, C.V., Aleo, S.J., Zanna, C., Roberti, M., Scandiffio, L., Loguercio Polosa,
762 P., Fiori, J., Porru, E., Roda, A., Carelli, V., et al. (2020). Fine-tuning of the
763 respiratory complexes stability and supercomplexes assembly in cells defective of
764 complex III. Biochim Biophys Acta Bioenerg *1861*, 148133.
765 10.1016/j.bbabio.2019.148133.
766 79. Kovarova, N., Pecina, P., Nuskova, H., Vrbacky, M., Zeviani, M., Mracek, T.,
767 Viscomi, C., and Houstek, J. (2016). Tissue- and species-specific differences in
768 cytochrome c oxidase assembly induced by SURF1 defects. Biochim Biophys Acta
769 *1862*, 705-715. 10.1016/j.bbadis.2016.01.007.
770 80. Cox, J., and Mann, M. (2008). MaxQuant enables high peptide identification rates,
771 individualized p.p.b.-range mass accuracies and proteome-wide protein
772 quantification. Nat Biotechnol *26*, 1367-1372. 10.1038/nbt.1511.
773 81. Brischigliaro, M., Frigo, E., Fernandez-Vizarra, E., Bernardi, P., and Viscomi, C.
774 (2022). Measurement of mitochondrial respiratory chain enzymatic activities in
775 Drosophila melanogaster samples. STAR Protoc *3*, 101322.
776 10.1016/j.xpro.2022.101322.
777 82. Fernandez-Vizarra, E., and Zeviani, M. (2021). Blue-Native Electrophoresis to
778 Study the OXPHOS Complexes. In Mitochondrial Gene Expression: Methods and
779 Protocols, M. Minczuk, and J. Rorbach, eds. (Springer US), pp. 287-311.
780 10.1007/978-1-0716-0834-0_20.
781 83. Brischigliaro, M., Cabrera-Orefice, A., Sturlese, M., Elurbe, D.M., Frigo, E.,
782 Fernandez-Vizarra, E., Moro, S., Huynen, M.A., Arnold, S., Viscomi, C., and
783 Zeviani, M. (2022). CG7630 is the Drosophila melanogaster homolog of the
784 cytochrome c oxidase subunit COX7B. EMBO Rep *23*, e54825.
785 10.15252/embr.202254825.
786 84. Giese, H., Ackermann, J., Heide, H., Bleier, L., Drose, S., Wittig, I., Brandt, U., and
787 Koch, I. (2015). NOVA: a software to analyze complexome profiling data.
788 Bioinformatics *31*, 440-441. 10.1093/bioinformatics/btu623.

789 85. Guerrero-Castillo, S., Baertling, F., Kownatzki, D., Wessels, H.J., Arnold, S., Brandt,
790 U., and Nijtmans, L. (2017). The Assembly Pathway of Mitochondrial Respiratory
791 Chain Complex I. Cell Metab *25*, 128-139. 10.1016/j.cmet.2016.09.002.
792 86. van Strien, J., Haupt, A., Schulte, U., Braun, H.P., Cabrera-Orefice, A., Choudhary,
793 J.S., Evers, F., Fernandez-Vizarra, E., Guerrero-Castillo, S., Kooij, T.W.A., et al.
794 (2021). CEDAR, an online resource for the reporting and exploration of
795 complexome profiling data. Biochim Biophys Acta Bioenerg *1862*, 148411.
796 10.1016/j.bbabio.2021.148411.
797
798

FIGURE CAPTIONS

Figure 1. *D. melanogaster* mitochondrial respiratory chain does not rely on SC formation under physiological conditions. (A) Complexome profiling of wild-type *D. melanogaster* mitochondria. Heatmaps show relative abundance of MRC subunits belonging to complex I (CI), complex II (CII), complex III_2 (CIII) and complex IV (CIV). Color scale of normalized peptide intensities are 0 (black), 96th percentile (yellow) and 1 (red). **(B)** BN-PAGE separation of mitochondria from wild-type *D. melanogaster* solubilized with digitonin. Native gels were either stained with Coomassie R250 or analyzed by in-gel activity (IGA) for complex I (CI) and complex IV (CIV). **(C)** BN-PAGE separation of mitochondria from wild-type *D. melanogaster* solubilized with dodecylmaltoside (DDM). Native gels were either stained with Coomassie R250 or analyzed by in-gel activity assay (IGA) for complex I (CI) and complex IV (CIV).

Figure 2. Severely perturbed CIV assembly results in increased formation of SC I_1III_2. (A) Complexome profiling of Coa8 KO *D. melanogaster* mitochondria. Heatmaps show relative abundance of MRC subunits belonging to complex I (CI), complex II (CII), complex III_2 (CIII) and complex IV (CIV). Color scale of normalized peptide intensities are 0 (black), 96° percentile (yellow) and 1 (red). **(B)** Average MS profiles depicted as relative abundance of MRC enzymes in natively separated complexes from wild-type (top) and Coa8 KO (bottom) fly mitochondria. Profiles of complexes I, III_2 and V (CI, CIII and CV) are plotted as average peptide intensity of the specific subunits identified by MS for each complex vs. apparent molecular weight. The increase in the relative abundance of SC I_1III_2 in Coa8 KO mitochondria is indicated by a black arrow. **(C)** In gel-activity assays for MRC complex I (CI), complex II (CII) and complex IV (CIV) in DDM-solubilized mitochondria from wild-type (w^{1118}) and Coa8 KO ($Coa8^{KO}$) flies. **(D)** BN-PAGE, western blot immunodetection of MRC complexes from wild-type (w^{1118}) and Coa8 KO ($Coa8^{KO}$) fly mitochondria using antibodies against specific subunits: anti-UQCRC2 (complex III), anti-NDUFS3 (complex I), anti-COX4 (complex IV) and anti-SDHA (complex II).

Figure 3. Mildly perturbed CIV assembly results in increased formation of SC I_1III_2. (A) Relative quantification (RQ) of *Coa8* mRNA expression in control (*da-gal4*>+) and *Coa8* KD (*da-gal4*>$Coa8^{RNAi}$) flies measured by qPCR. Data are plotted as mean ± SD ($n = 3$ biological replicates, Student's t test $*p \leq 0.05$). **(B)** In gel-activity assays for MRC complex I (CI), complex II (CII) and complex IV (CIV) in DDM-solubilized mitochondria

from control (*da-gal4*>+) and *Coa8* KD (*da-gal4>Coa8*^{RNAi}) flies. **(C)** BN-PAGE, western blot immunodetection of MRC complexes from a pool of three control (*da-gal4*>+) and three Coa8 KD (*da-gal4>Coa8*^{RNAi}) fly mitochondria samples, using antibodies against specific subunits: anti-UQCRC2 (complex III), anti-NDUFS3 (complex I), anti-COX4 (complex IV) and anti-SDHA (complex II).

Figure 4. Enhanced formation of SC I_1III_2 does not result in increased respiration. (A-B) High-resolution respirometry (HRR) analyses of whole-fly homogenates. Respiration is represented by oxygen flux (JO_2) measured by oxygen consumption rates (OCR – pmol/s*fly). OCR have been measured via substrate-driven respiration under saturating concentrations of substrates inducing either complex I (CI) or complex II (CII) -linked respiration. Rotenone was used to block CI-linked respiration before measuring CII-linked respiration. HRR was performed on **(A)** *Coa8* KO and **(B)** *Coa8* KD fly homogenates compared to relative controls. Data are plotted as mean ± SD (n = 4 biological replicates). **(C-D)** Kinetic enzyme activity of individual MRC complexes in **(C)** *Coa8* KO and **(D)** *Coa8* KD compared with the relative control individuals, normalized by citrate synthase (CS) activity. Data are plotted as mean ± SD (n = 3 biological replicates, two-way ANOVA with Sidak's multiple comparisons, **$p \leq 0.01$, ****$p \leq 0.0001$).

Figure 5. Mild perturbation of $CIII_2$ biogenesis enhances SC formation in *D. melanogaster.* (A) Relative quantification (RQ) of *Bcs1* mRNA expression in control (*act5c-gal4*>+) and *Bcs1* KD (*act5c-gal4>Bcs1*^{RNAi}) larvae measured by qPCR. Data are plotted as mean ± SD (n = 3 biological replicates, Student's t test ***$p \leq 0.001$). **(B)** In gel-activity assays for MRC complex I (CI), complex II (CII) and complex IV (CIV) in DDM-solubilized mitochondria from control (*act5c-gal4*>+) and *Bcs1* KD (*act5c-gal4>Bcs1*^{RNAi}) larvae. **(C)** BN-PAGE, western blot immunodetection of MRC complexes from a pool of three control (*act5c-gal4*>+) and three *Bcs1* KD (*act5c-gal4>Bcs1*^{RNAi}) larvae mitochondria samples, using antibodies against specific subunits: anti-UQCRC2 (complex III), anti-NDUFS3 (complex I), anti-COX4 (complex IV) and anti-SDHA (complex II). **(D)** Kinetic enzyme activity of individual MRC complexes in control (*act5c-gal4*>+) and *Bcs1* KD (*act5c-gal4>Bcs1*^{RNAi}) larvae mitochondria normalized by citrate synthase (CS) activity. Data are plotted as mean ± SD (n = 3 biological replicates, two-way ANOVA with Sidak's multiple comparisons, **$p \leq 0.01$, ****$p \leq 0.0001$). **(E)** High-resolution respirometry (HRR) analyses of whole-fly homogenates. Respiration is represented by oxygen flux (JO_2)

measured by oxygen consumption rates (OCR – pmol/s*fly). OCR have been measured via substrate-driven respiration under saturating concentrations of substrates inducing either complex I (CI) or complex II (CII) -linked respiration. Rotenone was used to block CI-linked respiration before measuring CII-linked respiration. HRR was performed on control (*act5c-gal4*>+) and *Bcs1* KD (*act5c-gal4>Bcs1*^{RNAi}) homogenates compared to relative controls. Data are plotted as mean ± SD (n = 3 biological replicates, two-way ANOVA with Sidak's multiple comparisons, ****$p \leq 0.0001$). **(F)** Relative quantification (RQ) of *Bcs1* mRNA expression in control (*da-gal4*>+) and *Bcs1* KD (*da-gal4>Bcs1*^{RNAi}) larvae measured by qPCR. Data are plotted as mean ± SD (n = 3 biological replicates, Student's t test ***$p \leq 0.001$). **(G)** In gel-activity assays for MRC complex I (CI), complex II (CII) and complex IV (CIV) in DDM-solubilized mitochondria from control (*da-gal4*>+) and *Bcs1* KD (*da-gal4>Bcs1*^{RNAi}) larvae. **(H)** BN-PAGE, western blot immunodetection of MRC complexes from a pool of three control (*da-gal4*>+) and three *Bcs1* KD (*da-gal4>Bcs1*^{RNAi}) larvae mitochondria samples using antibodies against specific subunits: anti-UQCRC2 (complex III), anti-NDUFS3 (complex I), anti-COX4 (complex IV) and anti-SDHA (complex II). **(I)** Kinetic enzyme activity of individual MRC complexes in control (*da-gal4*>+) and *Bcs1* KD (*da-gal4>Bcs1*^{RNAi}) larvae mitochondria normalized by citrate synthase (CS) activity. Data are plotted as mean ± SD (n = 3 biological replicates, two-way ANOVA with Sidak's multiple comparisons, **$p \leq 0.01$). **(J)** High-resolution respirometric (HRR) analyses of whole-fly homogenates. Respiration is represented by oxygen flux (JO_2) measured by oxygen consumption rates (OCR - pmol/s*fly). OCR have been measured via substrate-driven respiration under saturating concentrations of substrates inducing either complex I (CI) or complex II (CII) -linked respiration. Rotenone was used to block CI-linked respiration before measuring CII-linked respiration. HRR was performed on control (*act5c-gal4*>+) and *Bcs1* KD (*act5c-gal4>Bcs1*^{RNAi}) homogenates compared to relative controls. Data are plotted as mean ± SD (n = 3 biological replicates, two-way ANOVA with Sidak's multiple comparisons, ****$p \leq 0.0001$).

Figure 6. Mild perturbation of CI biogenesis enhances SC formation in *D. melanogaster.* (A) Relative quantification (RQ) of *Ndufs4* mRNA expression in control (*act5c-gal4*>+) and *Ndufs4* KD (*act5c-gal4>Ndufs4*^{RNAi}) larvae measured by qPCR. Data are plotted as mean ± SD (n = 3 biological replicates, Student's t test **$p \leq 0.01$). **(B)** In gel-activity assays for MRC complex I (CI), complex II (CII) and complex IV (CIV) in DDM-solubilized mitochondria from control (*act5c-gal4*>+) and *Ndufs4* KD (*act5c-*

902 *gal4>Ndufs4*^{RNAi}) larvae. **(C)** BN-PAGE, western blot immunodetection of MRC complexes
903 from a pool of three control (*act5c-gal4*>+) and three *Ndufs4* KD (*act5c-gal4>Ndufs4*^{RNAi})
904 larvae mitochondria samples, using antibodies against specific subunits: anti-UQCRC2
905 (complex III), anti-NDUFS3 (complex I), anti-COX4 (complex IV) and anti-SDHA (complex
906 II). **(D)** Kinetic enzyme activity of individual MRC complexes in control (*act5c-gal4*>+) and
907 *Ndufs4* KD (*act5c-gal4>*^{RNAi}) larvae mitochondria normalized by citrate synthase (CS)
908 activity. Data are plotted as mean ± SD (n = 3 biological replicates, two-way ANOVA with
909 Sidak's multiple comparisons, **$p \leq 0.01$, ***$p \leq 0.001$). **(E)** High-resolution respirometry
910 (HRR) analyses of whole-fly homogenates. Respiration is represented by oxygen flux
911 (JO_2) measured by oxygen consumption rates (OCR – pmol/s*fly). OCR have been
912 measured via substrate-driven respiration under saturating concentrations of substrates
913 inducing either complex I (CI) or complex II (CII) -linked respiration. Rotenone was used to
914 block CI-linked respiration before measuring CII-linked respiration. HRR was performed on
915 control (*act5c-gal4*>+) and *Ndufs4* KD (*act5c-gal4>Ndufs4*^{RNAi}) homogenates compared to
916 relative controls. Data are plotted as mean ± SD (n = 3 biological replicates, two-way
917 ANOVA with Sidak's multiple comparisons, ****$p \leq 0.0001$). **(F)** Relative quantification (RQ)
918 of *Ndufs4* mRNA expression in control (*da-gal4*>+) and *Ndufs4* KD (*da-gal4>Ndufs4*^{RNAi})
919 larvae measured by qPCR. Data are plotted as mean ± SD (n = 3 biological replicates,
920 Student's t test ***$p \leq 0.001$). **(G)** In gel-activity assays for MRC complex I (CI), complex II
921 (CII) and complex IV (CIV) in DDM-solubilized mitochondria from control (*da-gal4*>+) and
922 *Ndufs4* KD (*da-gal4>Ndufs4*^{RNAi}) larvae. **(H)** BN-PAGE, western blot immunodetection of
923 MRC complexes from a pool of three control (*da-gal4*>+) and three *Ndufs4* KD (*da-*
924 *gal4>Ndufs4*^{RNAi}) larvae mitochondria samples, using antibodies against specific subunits:
925 anti-UQCRC2 (complex III), anti-NDUFS3 (complex I), anti-COX4 (complex IV) and anti-
926 SDHA (complex II). **(I)** Kinetic enzyme activity of individual MRC complexes in control (*da-*
927 *gal4*>+) and *Ndufs4* KD (*da-gal4>Ndufs4*^{RNAi}) larvae mitochondria normalized by citrate
928 synthase (CS) activity. Data are plotted as mean ± SD (n = 3 biological replicates, two-way
929 ANOVA with Sidak's multiple comparisons, *$p \leq 0.05$). **(J)** High-resolution respirometry
930 (HRR) analyses of whole-fly homogenates. Respiration is represented by oxygen flux
931 (JO_2) measured by oxygen consumption rates (OCR - pmol/s*fly). OCR have been
932 measured via substrate-driven respiration under saturating concentrations of substrates
933 inducing either complex I (CI) or complex II (CII) -linked respiration. Rotenone was used to
934 block CI-linked respiration before measuring CII-linked respiration. HRR was performed on
935 control (*act5c-gal4*>+) and *Ndufs4* KD (*act5c-gal4>*^{RNAi}) homogenates compared to

936 relative controls. Data are plotted as mean ± SD (n = 4 biological replicates, two-way
937 ANOVA with Sidak's multiple comparisons).
938

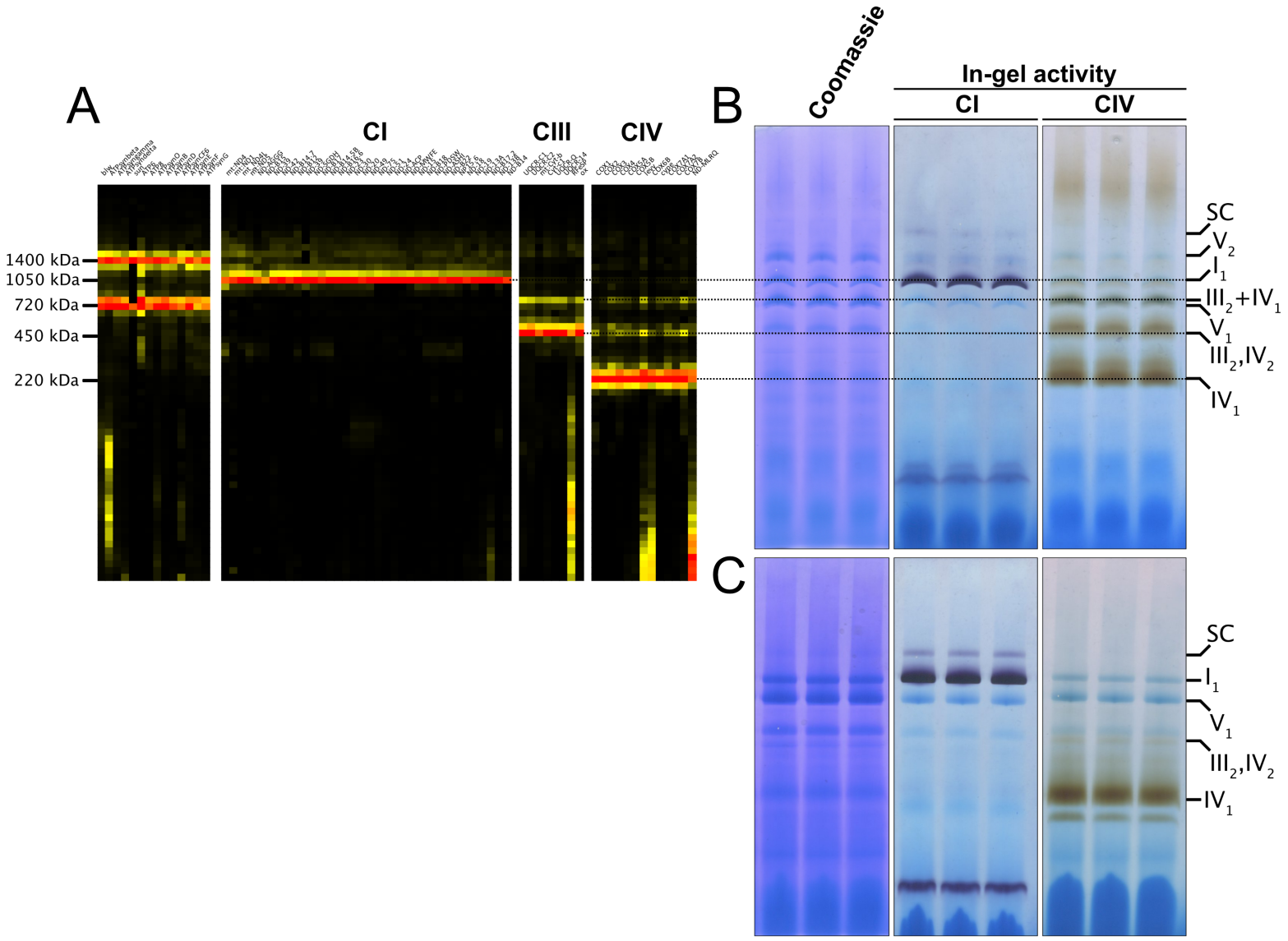
A
CI
CIII
CIV
1400 kDa
1050 kDa
720 kDa
450 kDa
220 kDa
B
Coomassie
In-gel activity
CI
CIV
SC
V2
I1
III2+IV1
V1
III2,IV2
IV1
C
SC
I1
V1
III2,IV2
IV1

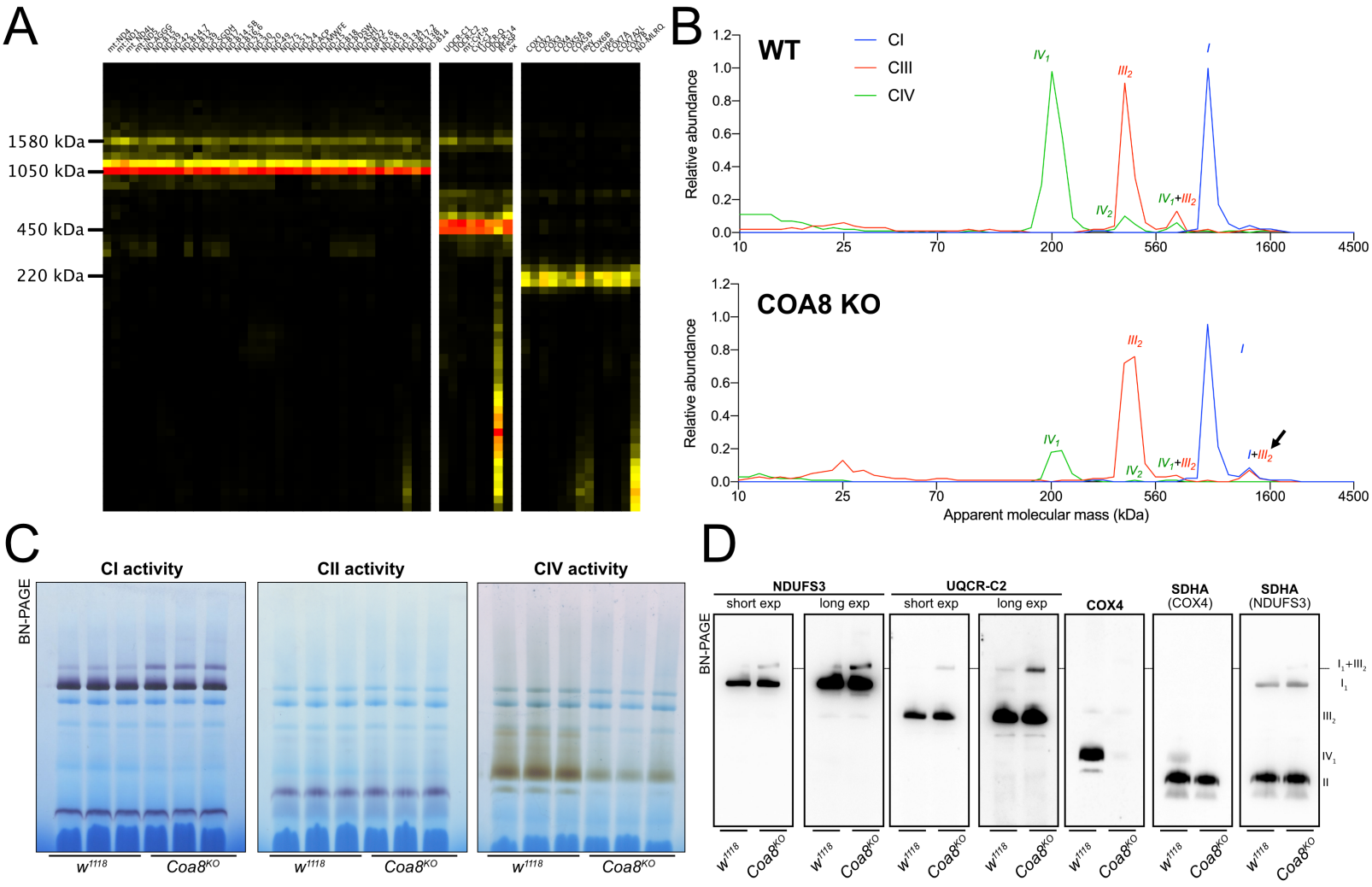
A
1580 kDa
1050 kDa
450 kDa
220 kDa
B
WT
CI
CIII
CIV
Relative abundance
COA8 KO
Apparent molecular mass (kDa)
C
CI activity
CII activity
CIV activity
BN-PAGE
w1118
Coa8KO
D
NDUFS3
UQCR-C2
short exp
long exp
COX4
SDHA (COX4)
SDHA (NDUFS3)
BN-PAGE

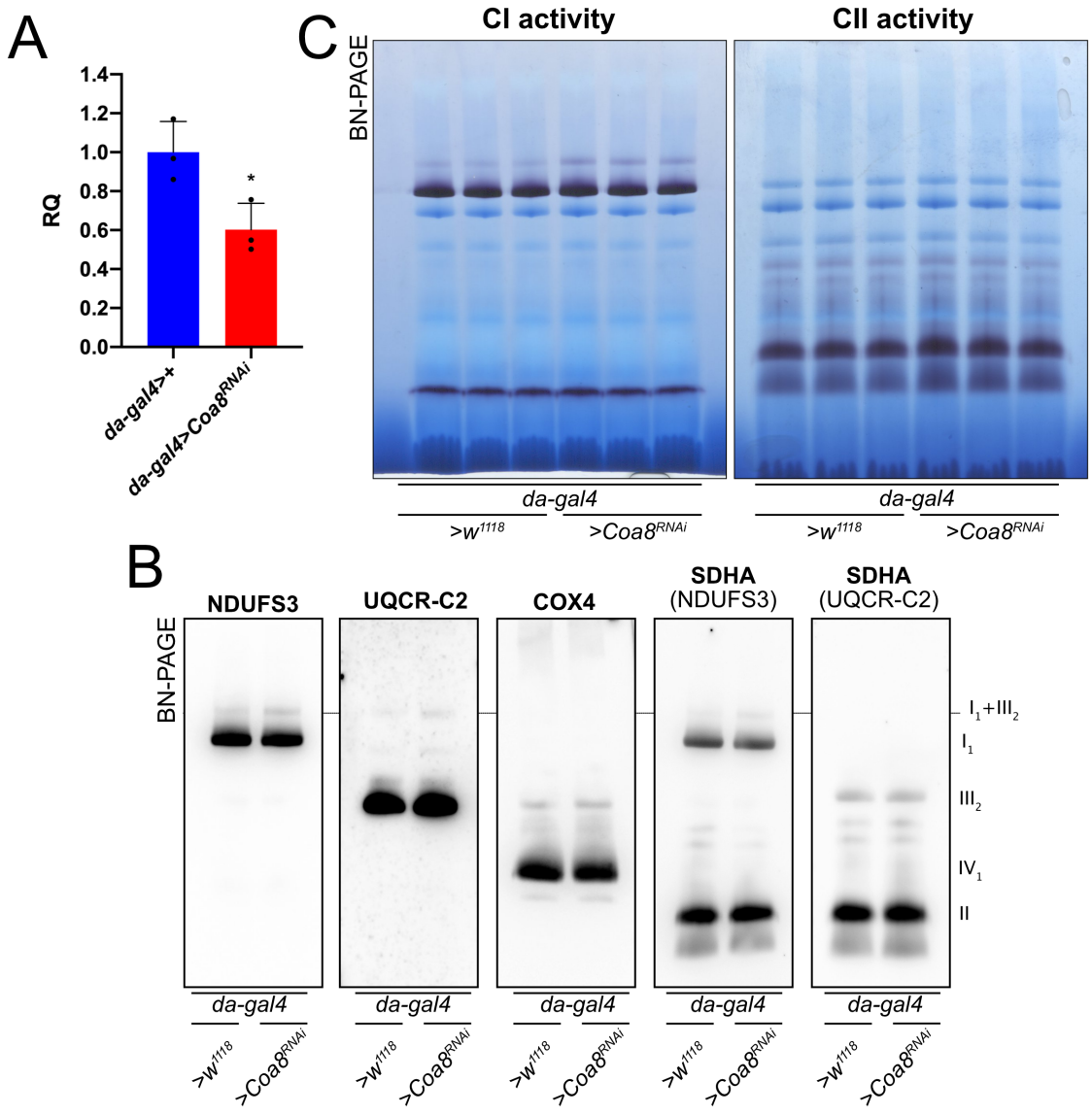
A
RQ
1.4
1.2
1.0
0.8
0.6
0.4
0.2
0.0
*
da-gal4>+
da-gal4>Coa8RNAi
C
CI activity
CII activity
BN-PAGE
da-gal4
>w1118
>Coa8RNAi
B
NDUFS3
UQCR-C2
COX4
SDHA (NDUFS3)
SDHA (UQCR-C2)
BN-PAGE
I1+III2
I1
III2
IV1
II
da-gal4
>w1118
>Coa8RNAi

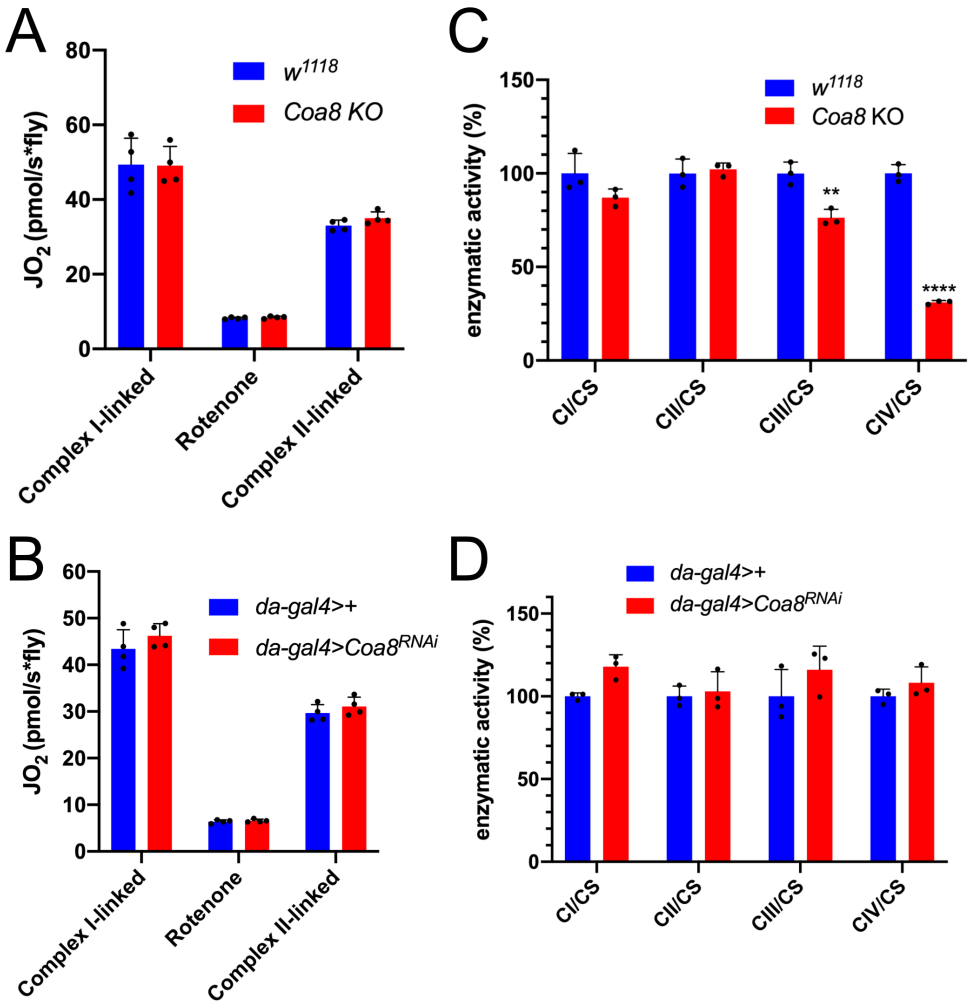
A
80
60
40
20
0
JO2 (pmol/s*fly)
w1118
Coa8 KO
Complex I-linked
Rotenone
Complex II-linked
C
150
100
50
0
enzymatic activity (%)
w1118
Coa8 KO
**
****
CI/CS
CII/CS
CIII/CS
CIV/CS
B
60
50
40
30
20
10
0
JO2 (pmol/s*fly)
da-gal4>+
da-gal4>Coa8RNAi
Complex I-linked
Rotenone
Complex II-linked
D
150
100
50
0
enzymatic activity (%)
da-gal4>+
da-gal4>Coa8RNAi
CI/CS
CII/CS
CIII/CS
CIV/CS

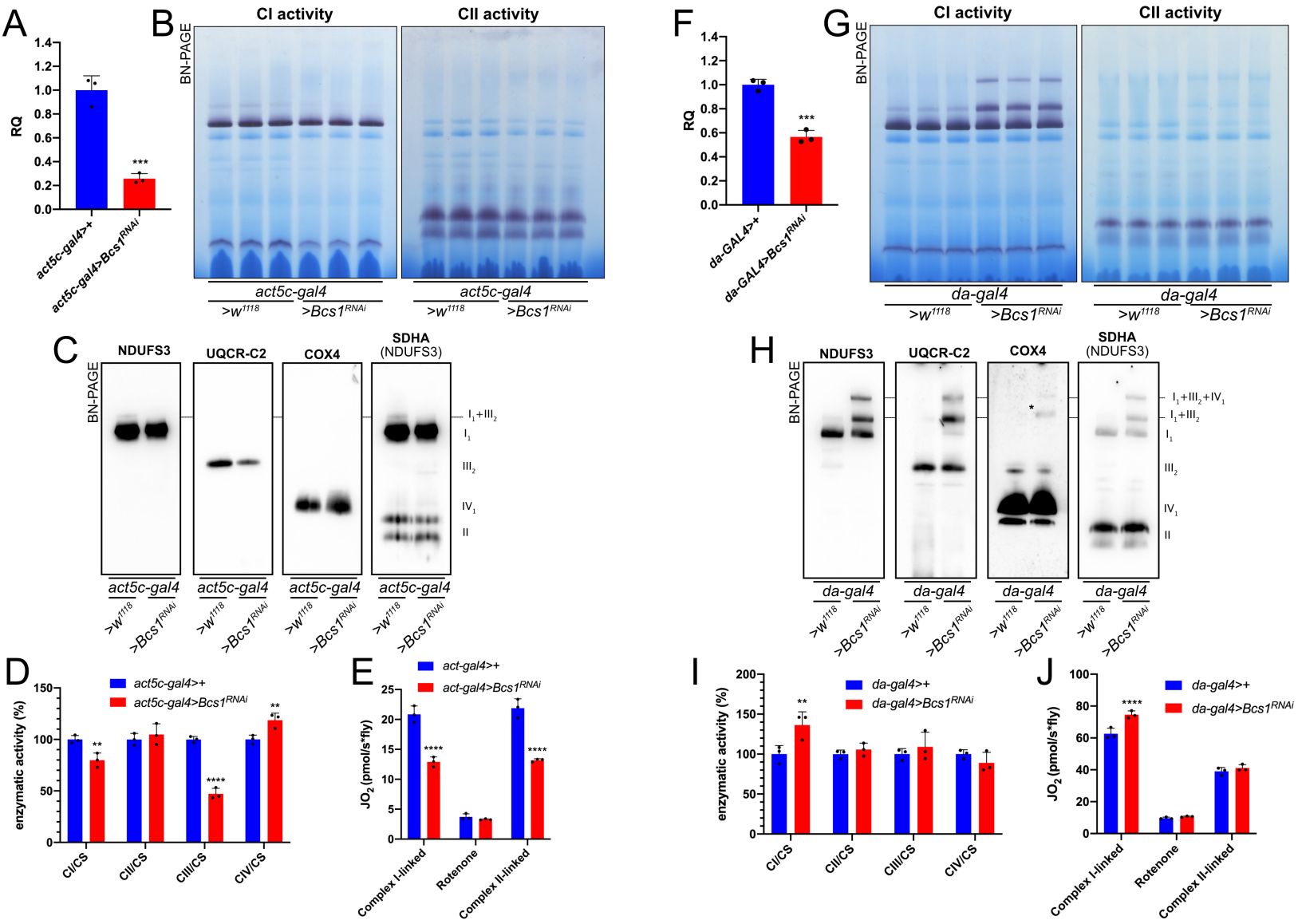
A
RQ
act5c-gal4>+
act5c-gal4>Bcs1RNAi
B
BN-PAGE
CI activity
CII activity
act5c-gal4
>w1118
>Bcs1RNAi
C
NDUFS3
UQCR-C2
COX4
SDHA (NDUFS3)
I1+III2
I1
III2
IV1
II
D
act5c-gal4>+
act5c-gal4>Bcs1RNAi
enzymatic activity (%)
CI/CS
CII/CS
CIII/CS
CIV/CS
E
act-gal4>+
act-gal4>Bcs1RNAi
JO2 (pmol/s*fly)
Complex I-linked
Rotenone
Complex II-linked
F
da-GAL4>+
da-GAL4>Bcs1RNAi
G
da-gal4
H
I1+III2+IV1
I
da-gal4>+
da-gal4>Bcs1RNAi
J

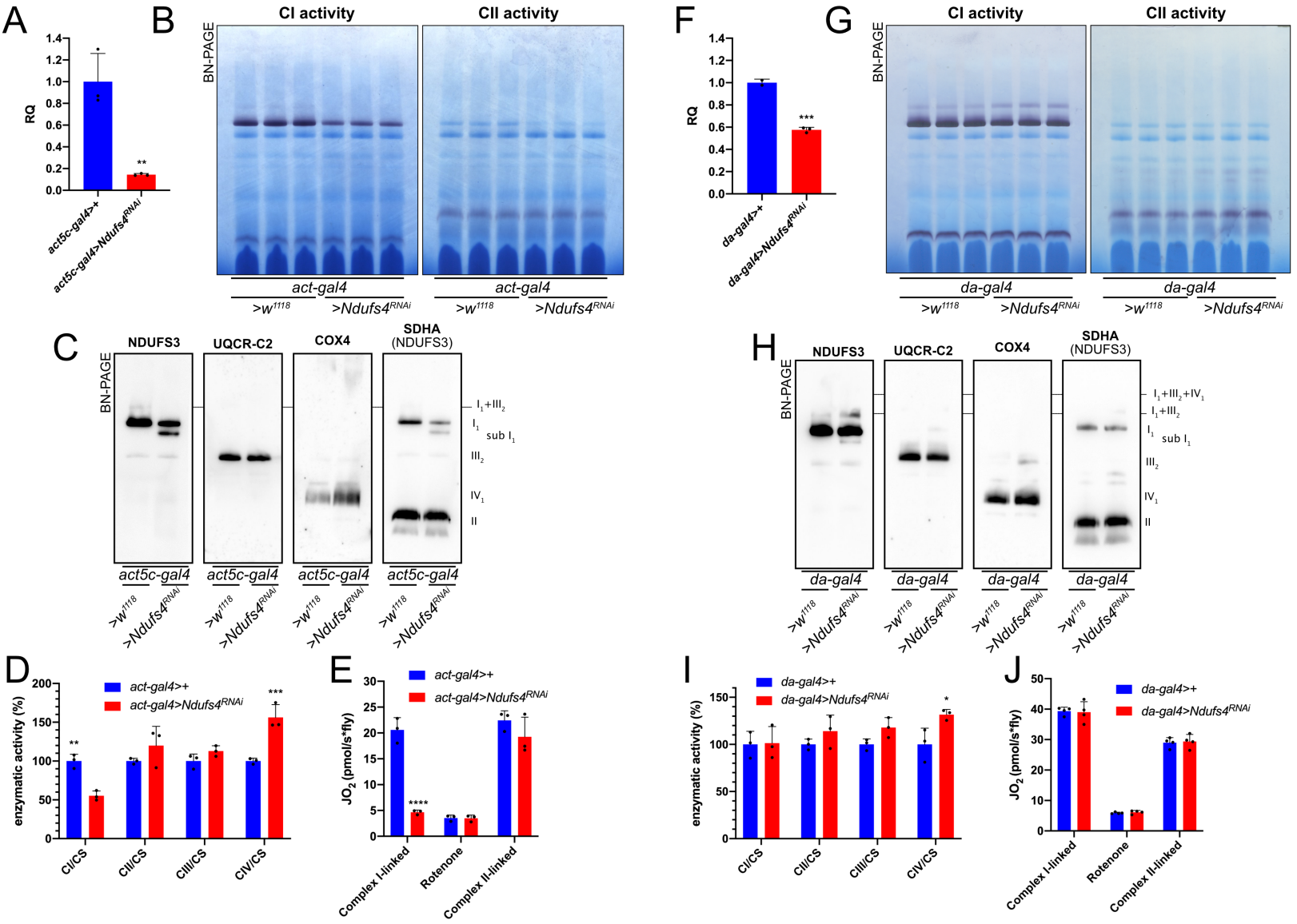
A
RQ
act5c-gal4>+
act5c-gal4>Ndufs4RNAi
B
CI activity
CII activity
BN-PAGE
act-gal4
>w1118
>Ndufs4RNAi
C
NDUFS3
UQCR-C2
COX4
SDHA (NDUFS3)
BN-PAGE
I1+III2
I1
sub I1
III2
IV1
II
act5c-gal4
>w1118
>Ndufs4RNAi
D
enzymatic activity (%)
act-gal4>+
act-gal4>Ndufs4RNAi
CI/CS
CII/CS
CIII/CS
CIV/CS
E
JO2 (pmol/s*fly)
Complex I-linked
Rotenone
Complex II-linked
F
da-gal4>+
da-gal4>Ndufs4RNAi
G
da-gal4
H
I1+III2+IV1
I
J